Mujezinovic Semir BSc

PHYSICS BASED TRANSMISSION RAIL CONTROL MODELLING AND CONTROL

MASTER THESIS

to achieve the University degree of Master of Science

Master degree programme: Mechanical Engineering

submitted to

Graz University of Technology

Supervisor

Associate Prof. Dr. Mario Hirz

Institute of Automotive Engineering

MSc. Sandor Kotan

AVL List

Graz, May 2018

Acknowledgement

To my parents who gave everything for me to have the opportunity to see the world. To my girlfriend for being there for me and support me and to all my friends that were part of this journey.

Affidavit

I declare that I have authored this thesis independently, that I have not used other than the declared sources/resources, and that I have explicitly indicated all material which has been quoted either literally or by content from the sources used. The text document uploaded to TUGRAZonline is identical to the present master thesis.

Date	Signature

Abstract

In the thesis, the rail with fork for gear preselection and engagement in dual clutch transmission (DCT) was investigated. The physical laws that occur during these processes were described, whereby only the gear preselection in DCT, which occurs on the clutch side that is opened has been considered. The engagement itself occurred through movement of the rail with fork. The rail further moved the synchronizers while the electro-hydraulic or electric actuator force and the position of the rail are controlled. The current plant model and controller were made with a certain consideration of the dynamics of the system for the rail movement. Through rail position and the predefined time needed for synchronisation and synchronizers capacity, the gear engagement was controlled. Through literature study, dynamic equations were obtained. Four main phases of the synchronization process control were considered. Simplifications of the dynamic equations were taken. The Simulink control model was developed for the gear engagement, starting from the neutral position, according to the simplified equations for each of those phases. In addition, a new control proposal of each phase was developed and one novel preselect shift strategy was proposed in DCT for the wear reduction of the synchronizers and to increase the durability of the gearbox.

Kurzfassung

Die Masterarbeit “Physics based rail model and control” (“Physikalisches Model der Schaltgabel und der Steuerung“) beschäftigt sich mit der Analyse der Vorwahl des Ganges bei Doppelkupplungsgetrieben (DCT). Bei der Analyse wurden die physikalischen Gesetze, die den Prozess der Vorwahl beeinflussen, untersucht, wobei die Vorwahl im lastfreien Zweig des Doppelkupplungsgetriebes berücksichtigt wurde. Durch die Bewegung der Schaltgabel wurde der Vorwahlvorgang eingeleitet. Die Schaltgabel leitet die Schaltkraft über die Synchronisationseinheit weiter. Die Bewegung der Schaltgabel wurde in den betrachteten Systemen durch den elektro-hydraulischen oder elektrischen Aktuator durch die Einleitung der Schaltkraft gesteuert, wobei die Position der Schaltgabel berücksichtigt wurde. Die Steuerungseinheit des DCT wurde näherungsweise ohne die genaue Analyse des dynamischen Systems programmiert, wobei in der Entwicklung der Steuerung ein Fokus auf die Position der Schaltgabel, die vorgewählte Synchronisationzeit und die Kapazität des Synchronringes gelegt wurde. Aus der Literatur wurden die Vorwahlgleichungen und die Vorwahlphasen entnommen und hinsichtlich der Aufgabenstellung analysiert. Schließlich wurde mit Hilfe von MATLAB Simulink ein Modell erstellt, welches die Schaltgabel bei der Vorwahl eines Ganges simuliert. Des Weiteren wurde ein neuer Ansatz zur Steuerung der verschiedenen Schaltphasen vorgestellt und eine neuartige Vorwahlstrategie vorgeschlagen.

Contents

Nomenclature

a	Half width of a groove on the conical surface [m]
b	Half length of the cone generatrix [m]
F_{fork}	Axial shift force applied on the outer groove of the sleeve [N]
F_{spring}	Reaction force detent spring [N]
F_{BTL}	Break Through Load [N]
F_{BTL1}	Break Through Load from one strut detent[N]
F_{slr}	Fork self-locking resistance[N]
F_{fric}	Friction forces due to the sliding of the sleeve[N]
F_{fric_s}	Friction forces on the chamfer side between ring and sleeve teeth [N]
F_R	Friction force in the cone [N]
J_{sr}	Rotating inertia of synchro ring [$kg \cdot m^2$]
J_{geari}	Equivalent rotating inertia on the targeted gear [$kg \cdot m^2$]
J_{ii}	Rotating inertia of the corresponding gear [$kg \cdot m^2$]
J_{sl}	Rotating inertia of sliding sleeve [$kg \cdot m^2$]
k_{spring}	Spring rate [$\frac{N}{m}$]
K_{CC}	Form factor of the inner surface of synchro ring [$-$]
m_{sr}	Mass of synchro ring [kg]
m_{sl}	Mass of sliding sleeve [kg]
m_f	Mass of rail with fork [kg]
m_{sd}	Mass of strut detent [kg]
N_{sl}	Normal force, sleeve - strut detent [N]
N_{sr}	Normal force, sleeve - synchro ring [N]
N_{sd}	Normal force, strut detent - synchro ring [N]
N_c	Normal force, cone surfaces [N]
n_p	Number of struts [$-$]
n	Number of internal circumferential grooves on synchro ring [$-$]
R_{sl}	Mean effective radius on interlock gearing [m]
R_c	Mean cone radius [m]
T_{cd}	Clutch drag torque [$N \cdot m$]
T_I	Index torque [$N \cdot m$]
T_C	Frictional torque on cone surfaces [$N \cdot m$]
$T_{Cstatic}$	Frictional torque on cone surfaces [$N \cdot m$]
T_{fric}	Frictional torque on cone surfaces due to the friction in splines [$N \cdot m$]
x_{sl}	Axial displacement, sleeve [m]
x_{sd}	Axial displacement, strut detent [m]
$\dot{x}_{sl}$	Axial velocity, sleeve [$\frac{m}{s}$]
$\dot{x}_{sd}$	Axial velocity, strut detent [$\frac{m}{s}$]
$\ddot{x}_{sl}$	Axial acceleration, sleeve [$\frac{m}{s^2}$]
$\ddot{x}_{sd}$	Axial acceleration, strut detent [$\frac{m}{s^2}$]
y_{sd}	Radial displacement, strut detent [m]

$\dot{y}_{sd}$	Radial velocity, strut detent [$\frac{m}{s}$]
$\ddot{y}_{sd}$	Radial acceleration, strut detent [$\frac{m}{s^2}$]
$L_{spring,0}$	Spring length without load [m]
L_{spring}	Spring length when in neutral [m]
α_c	Cone angle [°]
β	Chamfer angle [°]
ω_{oc}	Angular velocity, opened clutch [$\frac{rad}{s}$]
ω_{cc}	Angular velocity, closed clutch [$\frac{rad}{s}$]
ω_{tg}	Angular velocity, target gear [$\frac{rad}{s}$]
ω_{sl}	Angular velocity, sleeve [$\frac{rad}{s}$]
$\dot{\omega}_{tg}$	Angular acceleration, target gear [$\frac{rad}{s^2}$]
$\dot{\omega}_{sl}$	Angular acceleration, sleeve [$\frac{rad}{s^2}$]
θ	Sleeve detent ramp angle [°]
μ_{sl}	Coefficient of friction, strut detent sleeve [−]
μ_c	Coefficient of friction, cone surfaces [−]
μ_{ch}	Coefficient of friction, chamfer [−]
μ	Oil dynamic viscosity [$\frac{N \cdot s}{m^2}$]
μ_{cd}	Clutch oil dynamic viscosity [$\frac{N \cdot s}{m^2}$]
μ_{solid}	Coefficient of friction, end of the mixed stage [−]
μ_v	Coefficient of friction, start of the mixed stage [−]
S_1	Stribeck's number, end of the mixed friction [−]
S_2	Stribeck's number, start of the mixed friction [−]
i_{cg}	Current gear ratio [−]
i_{tg}	Target gear ratio [−]
p	Pitch distance [mm]
$x_{sleeve_{stop1}}$	Switch condition phase 1 to phase 2 [m]
$x_{sleeve_{stop2}}$	Switch condition phase 3 to fly wheel [m]
$x_{sleeve_{stop3}}$	Switch condition phase 3 to phase 4 [m]
$x_{sleeve_{in}}$	Switch condition phase 4 to engaged [m]

1. Introduction

Currently different types of transmission are used in passenger vehicles. Most often multi-gear transmissions are applied in order to adapt the output of the internal combustion engine to the drive wheels. Those transmissions can be mainly divided into two categories: manual and automatic (1). Throughout history different types of gearbox were designed and developed, but nowadays most common used are (1), (2):

- Manual Transmission (MT):
  - Constant mesh transmission (unsynchronized)
  - Synchronized manual transmission
- Automatic Transmission (AT):
  - Automatic Manual Transmission (AMT)
  - Automatic planetary Transmission (AT)
  - Dual-Clutch Transmission (DCT)
- Continuously Variable Transmission (CVT).

The type of dual clutch transmission is the emphasis of this thesis. In recent development more vehicles are equipped with DCT (3). This type of transmission is also the latest of all these types that was introduced into the passenger vehicles (1). Detailed description about this type of transmission will be discussed in chapter 2.

1.1 Assignment

The goal of the Master Thesis "Physics Based Transmission Rail Control Model and Control" is to investigate the gear preselection and engagement in Dual Clutch Transmissions. Details about gear preselection process are discussed in chapter 2. The control possibility of this process is part of this investigation, while the controllable part of this process is the shift force for the movement of the shift rail with fork. While dual clutch transmissions can be understood as assembly of two manual transmissions, there are different but similar dynamics that influence the gear pre-engagement process. The goal of this thesis is to obtain the physical laws and equations for the gear pre-engagement and gear preselection mechanism movement and to model the control system in MATLAB Simulink, so that it can be used for the simulations of the gear shifting in dual clutch transmission. By obtaining the physical laws of the gear engagement, the possible control logic of the gear preselection should consider gear preselection failure and noise reduction.

1.2 Current state

Currently in dual clutch transmission, that was used as a case study for this thesis, simplified control model of the rail movement is implemented. The model is based on several threshold values without clear background of the system dynamics. Also the current MATLAB Simulink control model that represents the rail movement and the gear engagement is a non-physical model, where the emphasis of the time needed for the gear engagement was related to the actual rail position. The current model control was based

on actuator force, synchronizers capacity and predefined time for the synchronization. The rail control model simulated movement of rail pistons and the force applied on the rail. Furthermore, piston position and the force level were checked for different states in MATLAB Stateflow chart. Further discussion about MATLAB Stateflow can be found in chapter 5. Purpose of different states was to simulate synchronization process during gear preselection. With different force levels, synchronizer capacity, synchronization time and piston position, states were changed and the output was the successful or not successful gear engagement. With current model it was not possible to derive conclusions about possible gear teeth clashing or different delays during rail movement. Furthermore, the current model did not consider different gear inertia or clutch and other drag torques. The input values for the current model were the shift force, current driving condition, synchronizer capacity and time of the synchronization, while the piston position was observed.

1.3 Problems

Different literature, e.g. (4), (5), (6) and (7), addressed the problems and improvements within the gear shifting process in dual clutch transmissions, but very few of them investigated the problems occurring in the gear preselection process. Also these publications investigated the gear preselection strategy, which is not part of this thesis. In this thesis main topic is the problem that occurs during the movement of the gear preselection mechanism.

Even though the gear preselection process did not directly affect the gear shift quality, because it did not influence the gear shifting itself, the problems such as rattling noise and inability to engage gear or different engagement delays were the main issues of the gear preselection in DCT. These problems were the main scope of the rail control investigation (8).
Also, some car manufacturers had some problems with dual clutch transmissions in the past with mass-production car models (9).

2. Dual clutch transmission

2.1 Overview

Dual clutch transmissions can be understood as a combination of two manual gearboxes (10). In Figure 1 a simplified depiction of the similarities can be seen as on the left side (a) manual transmission and on the right side (b) dual clutch transmission are shown. In dual clutch transmission, one of the clutches is connected to one output shaft with the odd gears and the other one is connected with a second output shaft with the even gears (11). Comparing to manual transmissions, where the torque is interrupted during gear shifting, in dual clutch transmission there is not any torque interruption. This is possible, because gear shifting process in dual clutch transmissions happens through engaging one clutch and disengaging the other one at approximately same time (10), (12). Whereby, the other clutch had next possible gear already preselected.

Another difference to manual transmission, where dry clutches are standard in the passenger vehicles, dual clutch transmissions may also be equipped by wet clutches. In this master thesis, dual clutch transmission that was used for the study had wet clutches, whereby the dynamics of this DCT differed to the one with dry clutches. The DCT with wet clutches compared to the one with the dry clutches has lower efficiency due to the drag torque but has higher heat resistance, so it is more applicable for the high torque transfer (10), (13), (14), (15).

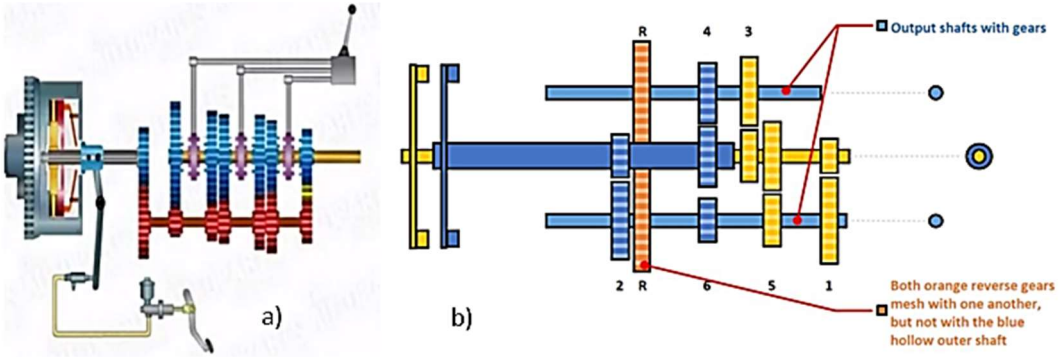

Figure 1 a) Manual transmission b) Dual clutch transmission (16) (17)

2.2 Gear shifting and preselection

Gear shifting in dual clutch transmissions with wet clutches is enabled by pressurizing the opened clutch with oil and depressurizing the closed clutch at the approximately same time, while the next gear, which is connected to the opened clutch, has already been preselected (13), (10).

The preselection process occurs always when the torque from the motor is not transferred and the clutch is fully opened (10). Figure 2 shows torque flow from the motor through transmission to the outputshaft as it was mentioned above.

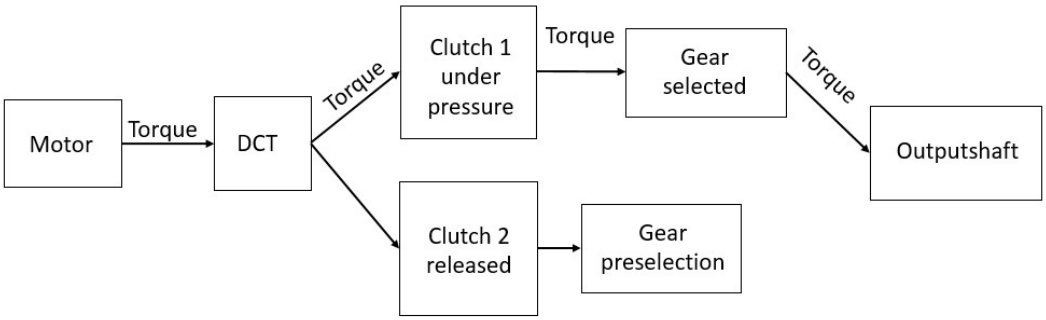

Figure 2 Torque flow

Gear preselection in dual clutch transmissions is the same process as gear shifting in manual transmissions, whereby the main difference is how the shift force is applied (18). In manual transmissions, the driver has the full control of the shift force that is applied on to the rail, while in DCT, the driver shifts by wire. In dual clutch transmissions, the driver does not have any influences on the shift force. Here, the control module has full control of the shifting process (2). The main parts of dual clutch transmission gear preselection mechanism, in this thesis also referred as the rails, are the shift rails with the forks, the actuators (hydraulic, electric etc.) and the synchronizer bodies (11).

In Figure 3 the scheme of the DCT that was part of this investigation is shown. As it can be seen, the clutch K1 is used for odd gears and K2 for even gears. For each gear pair 7-5, 3-1, R-4, 6-2 there is one rail that can engage gears during the preselection process.

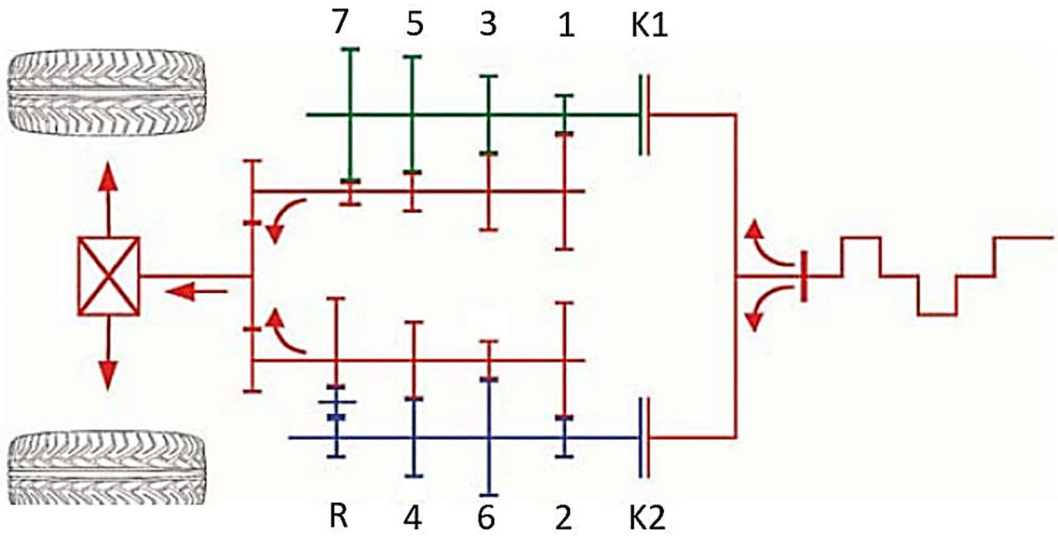

Figure 3 Investigated DCT scheme

2.3 Rail

2.3.1 Actuator

In dual clutch transmissions there are couple of possibilities to apply the shift force. The most common ones for wet clutches are electro-hydraulic actuators or fully electro-mechanic actuators (19).

Electro-hydraulic actuator is used in dual clutch transmission that was subject of this thesis. It consists of hydraulic pump, pressure line, solenoid valves, pressure control valves and actuating pistons with their chambers. The pressure for the shift force is created through the main pressure taken from the hydraulic line for the clutches (13).

Electro-mechanic actuators can also be used for gear preselection. One of the possibilities is characterized by an active interlock, where the electro-mechanic actuators consist of electric motor and shift selector with shift finger unit, as shown in Figure 4 (19).

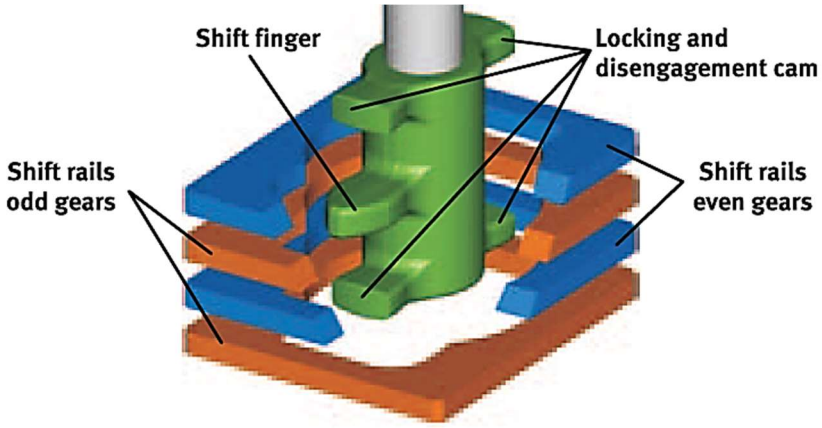

Figure 4 Shift rail selector with shift finger (19)

2.3.2 Shift rail with the fork

As already mentioned dual clutch transmission have lots of similarities with manual transmissions. Main difference comparing with the shift rail from the manual transmission is in the size and weight. The shift rail itself can be understood as metal cylinder (plate) where the metal fork is rigidly attached to. The main function for shift rail in DCT is the same as in manual transmission. It has to transfer the shift force from the actuator to synchronizer bodies. It should not be heavy and it should also be ensured that, due to the high dynamics of the system, it does not bend or damp the shift force. Figure 5 shows a shift rail with the fork and the pistons with the piston chambers of the electro-hydraulic actuators. In Figure 5 the locking sleeve is also illustrated. Its function is to hold the shift rail in neutral position without any pressure applied on the pistons and also to assist holding of the sleeve in the engaged position. This part has not the same design for every dual clutch transmission as it is illustrated here.

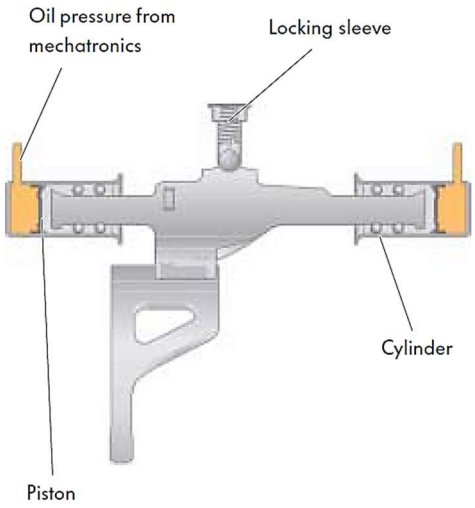

Figure 5 Rail with fork (11)

2.3.3 Synchronizer body

Most important part of rail is the synchronizer body. First developed synchronizer body was around 1920s with purpose to decrease gear shifting time in manual transmissions. The synchronizer body in DCT also called synchronizer has the same function and similar design as in manual transmissions. Different authors describe synchronizers for manual transmissions and their observations have also been included into this thesis, e.g. (1), (2), (10), (13).

Even though there are different designs of synchronizers, the function of the synchronizer body is same for all of them and that is to equalize the speed difference between the gear and the output shaft. In addition the function is to ensure gear coupling with the output shaft, so that the torque can be transferred to the differential (10). Figure 6 shows the shift rail with the fork and the connection to the synchronizer body.

Through history, different types of synchronizer bodies have been developed and constructed. They all had the same function that is mentioned above but they distinguished themselves in the design solutions. Some of the gearboxes used Lever-Type synchronizers, other Pin-Type but nowdays, the conventional Baulkring-Type is the most used for gear synchronisation processes (2).

This type of synchronisation body is also applied in dual clutch transmissions, that was used as a subject of this thesis. The Baulkring-Type can be seen in Figure 7, where one synchronizer body is assembled with one idler gear. According to the labels in Figure 7, the following parts are assemblrd in the synchronisation body (13):

1. Idler gear
2. Synchronizer gear hub with selector teeth and friction cone, which is part of the idler gear
3. Main part of the synchroniser body, synchronizer ring with counter-cone and locking teeth

4. Synchronizer inner body with internal teeth for positive locking with the transmission output shaft and external teeth for the sliding sleeve
5. Spring
6. Ball pin
7. Thrust piece
8. Gearshift sliding sleeve with internal teeth

The synchronizer gear hub and gear friction cone are either press fitted or laser welded with the gear wheel and they are fly wheeling together on the output shaft (2). On the synchronizer gear hub there are external teeth with chamfers on both sides that are used for the interlock with internal teeth of the sliding sleeve for gear engagement. The gear outer friction cone combined with the synchronizer ring inner friction cone is the heart of the synchronizer mechanism as their function is to match the speed of the gear with the speed of the sliding sleeve through friction torque for smooth and effortless gear engagement. The ball pin on a loaded spring with thrust piece is also called strut detent and is positioned between the groove in the synchro hub and the inner groove of the sliding sleeve. The number of strut detents in the synchronizer body can vary but usually there are only three of them. They have multiple functions as they are the first elements that generate load on the synchronizer ring through the movement of the sleeve as they hold the axial position of the sleeve teeth. Also this first load causes the small rotational rotation of the synchronizer ring within the recesses of the synchronization hub, where the strut detent are placed, so that it can get into the sleeve teeth blocking position (1), (10), (2).

In dual clutch transmissions there are several shift rails with synchronizers that can be moved in both directions, so that one synchroniser body can engage two different gears. In this thesis rail movement and control of the one rail moved in one direction toward the gear is discussed and investigated. As visible in Figure 5, the position sensor of the rail fork is also attached to the shift rail. On both ends of the shift rail there are bearings assembled to the shift rail so that the movement in axial direction is secured. In the synchronizers shown in these figures, there is only one cone set for speed synchronization, however, some of the synchronizer designs have more friction cones set up between the synchronizer ring and the gear synchronization cone as shown in Figure 8 with two red arrows pointing toward these cones. The purpose of these additional cones is to reduce the shift force needed for the synchronization process and on the other hand to increase the friction cone torque. In this thesis, synchronizer types with one cone area will be discussed in detail (20).

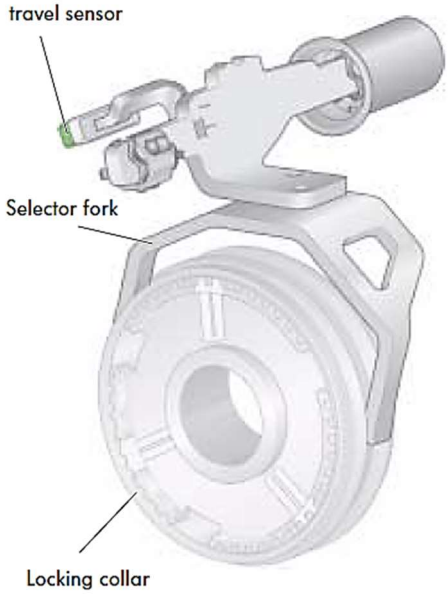

Figure 6 Rail with fork and synchronizer-body (11)

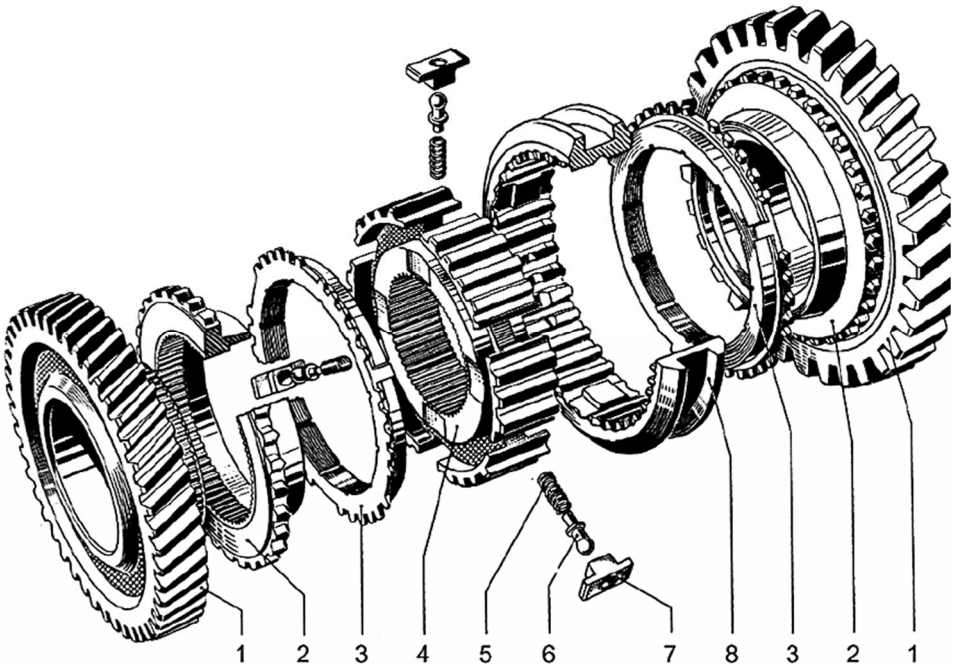

Figure 7 Synchronization-body (13)

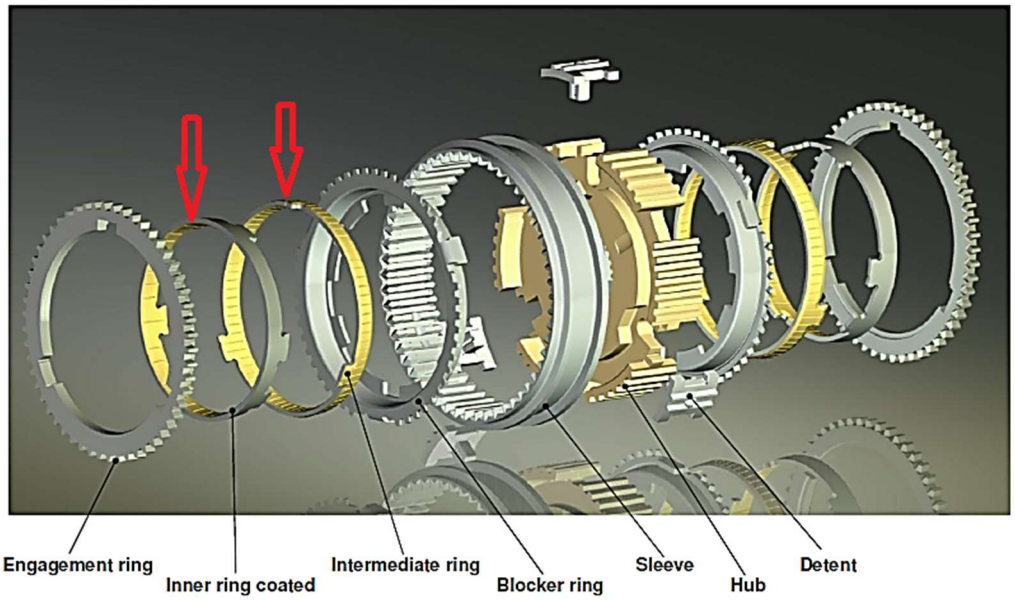

Figure 8 Synchronizer with more cones (20)

3. Rail-Physics

In previous chapter, main rail parts were introduced. In this chapter, interaction between different parts during rail movement will be discussed. Figure 9 shows interaction block diagram. In this diagram rail physics is divided into different phases that correspond to interactions between different rail parts during rail movement. Yellow arrows show connection between sleeve, strut-detent and synchronizer ring. Green arrows show connection between sleeve and synchronizer ring. Red arrows show connection between sleeve and targeted gear, while blue arrow shows that for certain part of rail movement sleeve and fork move without any significant interaction with other parts.

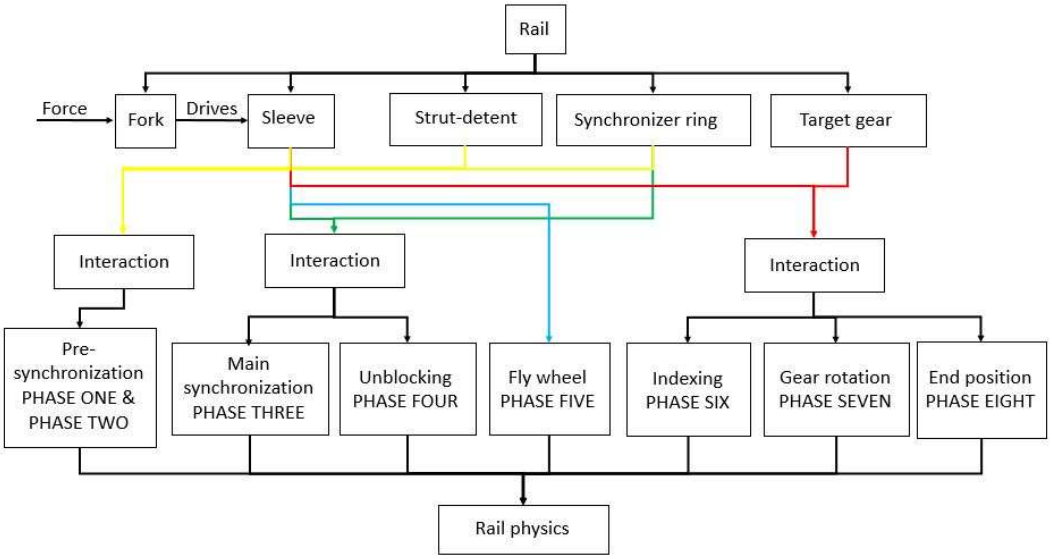

Figure 9 Interaction block diagram

In the present work, each rail assembly part has been taken under investigation. The interaction between each other and their contribution to the gear synchronisation and gear engagement were the main focus of investigations. The goal was to find the dynamic equations, based on physical laws, that could be used for modelling of the rail and also to understand what causes gear engagement noise and failures. Furthermore, through knowledge of the rail physics, possible control strategies of the gear preselection could be derived.

3.1 Actuator

The actuator that was used for gear preselection in the dual clutch transmission that was subject of this thesis is electro-hydraulic. This actuator uses the pressure from the main pressure line that is used for the clutch actuation. The shift force for the motion of the shift rail is created through the pressure applied on the double acting pistons that can move the rail in either direction (13). In this thesis, the focus was put on force level that was created by actuation. However, the actuation model and the dynamics of the actuator were not part of this thesis.

The mechatronic module, consisting of transmission control unit, hydraulic pressure, control pressure valves and on/off solenoid valve, controls the shift rail position through the actuation of the valves. Through filling of the piston chambers with oil, the pressure in one chamber would be higher than in the other chamber and through the pressure difference the shift rail movement would be achieved (13), (18).

Through the movement of the shift rail and also the pistons, volume variations of the piston chambers would occur, that could affect the shift force. Also the friction between the piston, shift rail and the piston chamber walls should be mentioned as parameters that can affect the shift force, but because of the high dynamics and the oil behaviour, these factors are neglected in this thesis.

3.2 Synchronization

The synchronization process is a highly nonlinear process, where through movement of the sliding sleeve over the synchronizer body hub, the synchronization and gear engagement are proceeded. Through the pressure increases in one piston chamber and decreases in the opposite one, the shift rail with the fork is moved axially in the needed direction as soon as the shift force is higher than the resistance forces (13).

The shift rail cannot be investigated as stand-alone part for the movement because as soon as the shift rail starts moving, through its connection with the synchronizer, different physical laws influence this movement according to synchronisation process. Most significant influence on the rail movement has the synchronizer body and the synchronization process. Different authors describe the synchronization process through different number of stages or phases, where different parts interact between each other and through that interaction different physical forces influence the rail movement and gear engagement, e.g. (1), (6), (10), (13), (14), (2).

The rail movement and the synchronization process can be described with eight different phases. Through different simplifications there is a possibility to describe the synchronization with only four phases, that can be further used for modelling of the synchronisation, rail movement and control model (10), (2), (15). All eight phases will be discussed and after the review of the mathematical models, a possible model simplification will be investigated and discussed.

3.2.1 Phase one and phase two

The first and second phase, also called pre-synchronization phases, begin just after the shift rail with the fork starts to move into the direction of the gear due to the rising oil pressure in one piston chamber. The pistons on both sides start to move and apply the force on the shift rail. This force is called shift force. The shift rail with the fork and the sleeve move all together axially, and the start of the first phase occurs while the sleeve, due to the contact from the sleeve and the ball pin under it, pushes the strut detent face to contact with the synchronizer ring. The end of the first phase is defined by the moment when the strut detent gets in contact with the synchronizer ring, but the synchronizer ring does not move towards the gear. The second phase starts just after the contact has been established and the strut detent starts pushing the synchronizer ring toward the gear. This phase is characterized by the building of a small oil film between the synchronizer ring cone and the gear cone. Due to the speed difference between the

gear and the synchronizer ring, small amount of the hydraulic cone friction torque is produced. This phase ends when the ball pin had travelled the length where the maximum resistance force from the detent spring against the rail movement would be applied on to the edge of the sleeve groove and stayed like that until phase three has not been started. Furthermore, at the end of phase two, the oil film between the chamfers of the synchronizer and sleeve teeth has been broken so that the ring and sleeve chamfers could get into contact (2).

The mechanical resistance forces are made of the kinetic and static friction forces between the ball and the inner sliding sleeve teeth and the mass of the sleeve and the shift rail with the fork. Through the oil behaviour, there is some damping effect, that can affect the movement of the rail (21).

In Figure 10 the neutral position on the left side is shown. Here, small distance between strut detent and synchro ring within red circle is notable. On the right side, the end of the first phase is shown as small movement of the sleeve and strut detent on the right side within the red circle are visible.

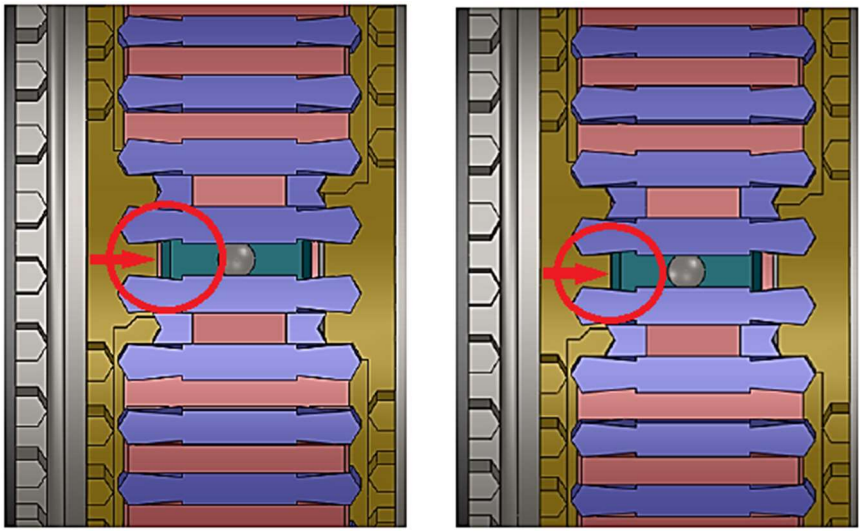

Figure 10 On the left side neutral position and on the right side strut detent contacts the ring (2)

3.2.2 Phase three

Due to the small amount of the hydraulic cone friction torque that has been created during pre-synchronization, in the phase three, also called angular synchronization, the synchronization ring rotates to the blocking position within the available space in the recesses of the synchronization hub, so that the sleeve axial movement is no longer possible. The chamfers of the sleeve teeth and the synchronisation ring teeth get in contact and the ring teeth block the further movement of the sleeve as long as the kinetic friction torque between gear and ring cone is larger than the indexing (blocking) torque created through the contact of the teeth chamfer of synchro ring and sleeve. Through the contact of the teeth chamfer of the synchronizer ring and the sleeve, the maximum force is applied onto the chamfer. This also means that the maximum of the cone friction torque is produced in this sequence. During this process the synchronizer ring heats itself and accordingly its effective cone diameter increases. Because of that

effect the synchroniser ring moves axially toward the gear. At the point when the speeds are synchronized and there is not any kinetic friction between the cones, the heat reduces quickly and the diameter of the ring cone reduces accordingly. Because the synchronizer ring is now in the position where the gear synchronization cone diameter is larger than the synchronizer ring cone, while the shift force is still applied on the synchronizer ring teeth chamfer, the ring might get stuck onto the gear synchronization cone and the kinetic friction might be transferred into static friction (2). This behaviour can be compared to the behaviour of friction clutches (10).

The phase three, shown in Figure 11, ends when the speed is synchronised and the ring sticks onto the gear cone, so that the sleeve can continue its axial movement. Position between sleeve teeth chamfer and ring chamfer as shown in this figure within the red circle, does not change during this phase.

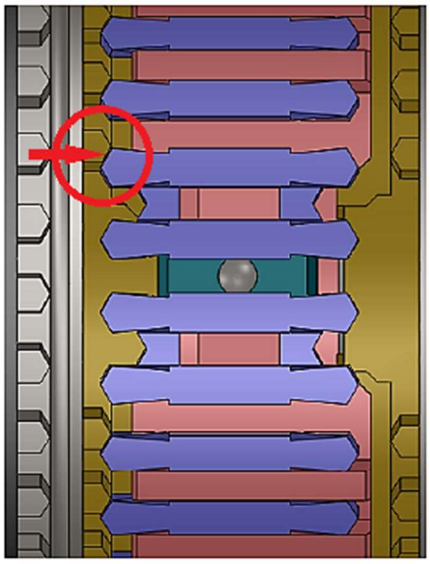

Figure 11 Phase 3 - Angular synchronization (2)

3.2.3 Phase four

Due to the static friction between the synchronizing ring and the gear synchronization cone the sleeve turns the gear and ring into a position so that the sleeve can continue its axial movement (2). It is also important to mention that some authors like (20) and (22), explain this phase only as if the ring will be turned backwards so that the sleeve would move forward, without influencing the gear rotation itself. As an enhancement, the case with rotation of both gear and ring is considered in this thesis. During this phase it is important that the indexing torque applied on the ring chamfer is higher than the drag torque that is transferred through the gear. The end of this phase is shown in Figure 12 within the red circle. After that, there is not any contact between the

chamfers of the synchronization ring teeth and the sliding sleeve inner teeth chamfer; thus the rotation phase of the ring has been finished.

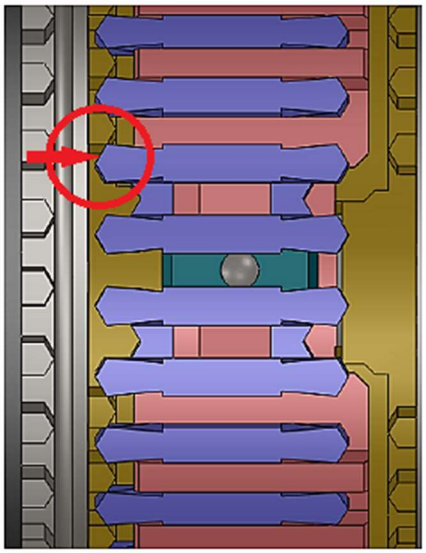

Figure 12 Phase 4 – Unblocking (2)

3.2.4 Phase five

After the ring has been turned, the sleeve teeth can move forward as the shift force is still applied. This phase is also called the second fly wheel phase, because there is almost no resistance for the movement of the sleeve. It is also very important that the fly-wheel phase is finished as soon as possible, because if drag torque in dual clutch transmission becomes higher than the static friction torque in the cone, the synchronisation ring would start slipping, what might further cause a speed difference of the sliding sleeve and the gear. This is an extremely sensitive phase for the gear engagement, because now the cold synchronization ring can be moved backwards into the neutral direction. Besides the friction between the sides of the synchronization and sliding sleeve teeth, the static friction in the cone and the small holding force of the strut detent, nothing else is holding the synchronization ring from sliding backwards from the static friction position, if the drag torque is higher than all of these forces combined together (10), (23).

In Figure 13 the phase five can be seen, where the end of the fly wheel phase is occurred when the contact between the gear synchronisation teeth chamfer with the sliding sleeve teeth chamfer has been established. Additionally, the movement resistance of the sleeve in this phase describes the physics behind the movement of the sleeve toward the neutral position from the engagement position.

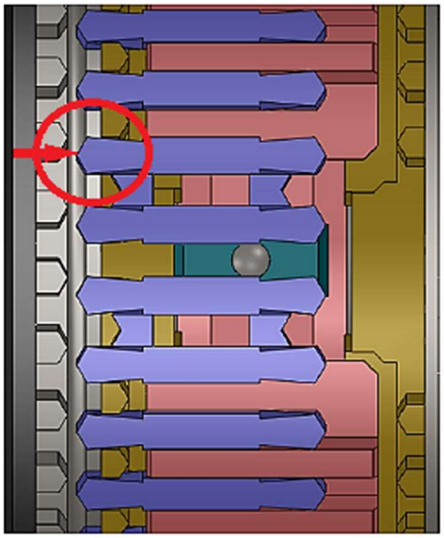

Figure 13 Phase 5 - Second Fly Wheel (2)

3.2.5 Phase six

The sixth phase is crucial for successful gear engagement. It is also called indexing phase. In this phase the relative position of the gear synchronization teeth to the position of the sliding sleeve teeth is very important (Figure 14). In this phase, the initial position of the gear synchronization teeth against the sliding sleeve teeth is defined randomly and there are couple of possible cases. First case is not having any contact between the chamfers of the gear synchronization teeth and the sliding sleeve teeth. Through the rotation of the synchronization ring, and such relative alignment of the sliding sleeve teeth and spacing between the gear synchronisation splines, it is possible to continue the fly wheel phase until gear engagement. For the second option, which is more likely, through the alignment after phase four, the chamfer teeth of the teeth will get into contact. Through this contact indexing torque will be produced. The indexing torque has to be applied on one hand to turn the gear and on the other hand to break the static friction connection of the cone clutches, because the ring has to be separated from the gear in order to turn the gear (21).

The phase six is shown with its starting position in Figure 15. Within red circle it is shown that the sleeve teeth chamfer and gear teeth chamfer are in contact. For this phase it is also important that the indexing torque that is created and controlled with the shift force is always larger than the drag torque. The last possible option, which is the least possible one, is that the sharpest parts of the teeth collide to each other. This will not be taken into consideration here. Due to the different design flaws, which will be discussed later, the possibility of this case is minimum (2), (24).

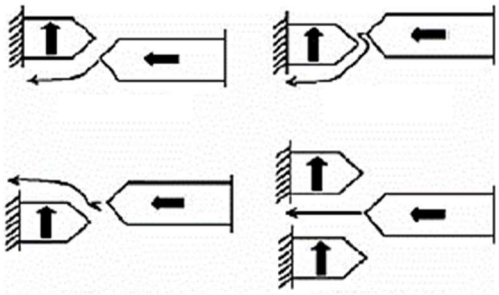

Figure 14 Teeth alignment (2)

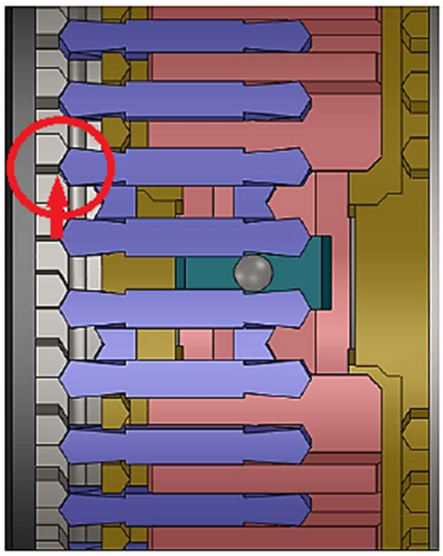

Figure 15 Phase 6 - Indexing (2)

3.2.6 Phase seven

In this phase the ring is separated from the gear cone clutch and the gear is turned and the sliding sleeve teeth are positioned in the space between the gear synchronisation teeth so that the gear engagement can be finished. Figure 16 shows the end position of the gear rotation.

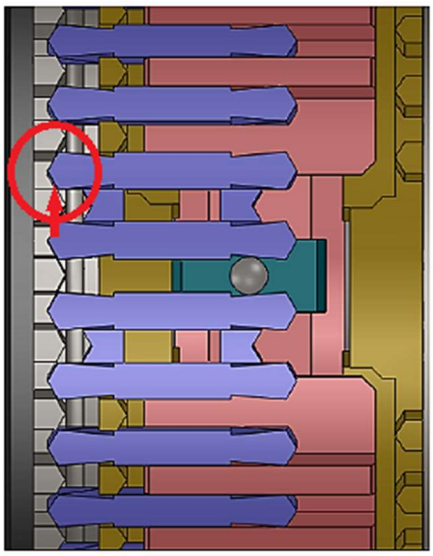

Figure 16 Phase 7 - Gear rotation (2)

3.2.7 Phase eight

As the sliding sleeve teeth have aligned within the space between the gear synchronization teeth for the gear engagement, the start of the final phase with different equations of motion would be initiated. Fast movement and short duration of this phase is necessary, as it could cause noise during the engagement. Noise might occur because when the gear is turned at the start of the final engagement there is not any controllable force that resists the drag torque. The contact between the sleeve and the gear teeth is only held by the sharp edges of the chamfers, while the gear cone and ring cone are separated. Several experimental data have been published, that it has been written that even though there is some slip in the cone and the speed difference it would be still possible to engage the gear without causing noise or , e.g. (15) (23).

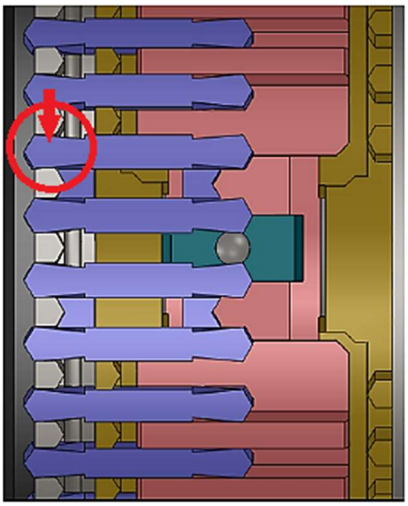

Figure 17 Phase 8 - Gear engagement (2)

3.3 Drag torque and vibrations

As already mentioned, the main reason for gear synchronisation problems and unsuccessful gear engagement is caused by too high drag torque and too low actuation forces after the fly wheel phase (1), (10), (2) , (23).

Drag torque is also a problem for gear synchronisation in manual transmission, but in dual clutch transmissions with wet clutches, it is more enhanced than in other transmission types due to the clutch drag torque. There are many limitations for the estimation of this torque, as there are different variables that are not measurable or there are different operating conditions, speed or temperature differences, that are subject of a high degree of variation. One of the authors also wrote about possible wrong synchronizer design assumptions, where in the synchronizer design process the drag torque in dual clutch transmission is estimated as too low. This could lead to the problems while synchronizing the gear speed with the output shaft speed and also due to the impossibility to match the speed if the drag torque is higher than the theoretically highest cone torque (14), (23). According to (23) following losses are combined as drag torque in dual clutch transmissions:

1. Bearing losses
2. Tooth friction losses
3. Gear windage losses
4. Clutch shear losses
5. Concentric shaft shear losses

The bearing losses and tooth friction losses are not different to those of manual transmissions; thus they will be not explained further. On the other side, the gear windage losses in dual clutch transmissions are defined as drag of the gear through its rotation in the air-oil mixture in the transmission. The clutch shearing torque and the viscous shearing torque caused by differential velocity in the open multi-plate wet clutch pack resist the direction of the motion. Specifically, for dual clutch transmission the shafts that connect the gear train with the clutches are always arranged concentric. Due to this arrangement, there are also viscous shearing losses between these two shafts, as there are bearings between them, which have to be lubricated (23). While all of these explained losses influence the gear change process, the clutch drag torque is strongly speed dependable and identified by various authors as the main problem of the gear synchronization process in dual clutch transmissions. In Figure 18 the schematics and the geometry of the opened clutch are shown. As mentioned in literature, due to the oil flow which is necessary for cooling in the clutches pack, there is significant amount of the torque transferred also through the opened clutch. The amount of the drag torque varies with the speed difference of the clutches. In Figure 19, the clutch drag behaviour over the speed difference of the clutches is shown for two different models that were developed from different literature. The Liu's model has shown itself as the more accurate one, because it calculates the drag torque in high speed difference more accurate (15), (25), (26), (23). The synchronization process in dual clutch transmissions is also exposed to the higher vibrations due to the fact that the gear engagement process occurs during the other clutch is closed (26).

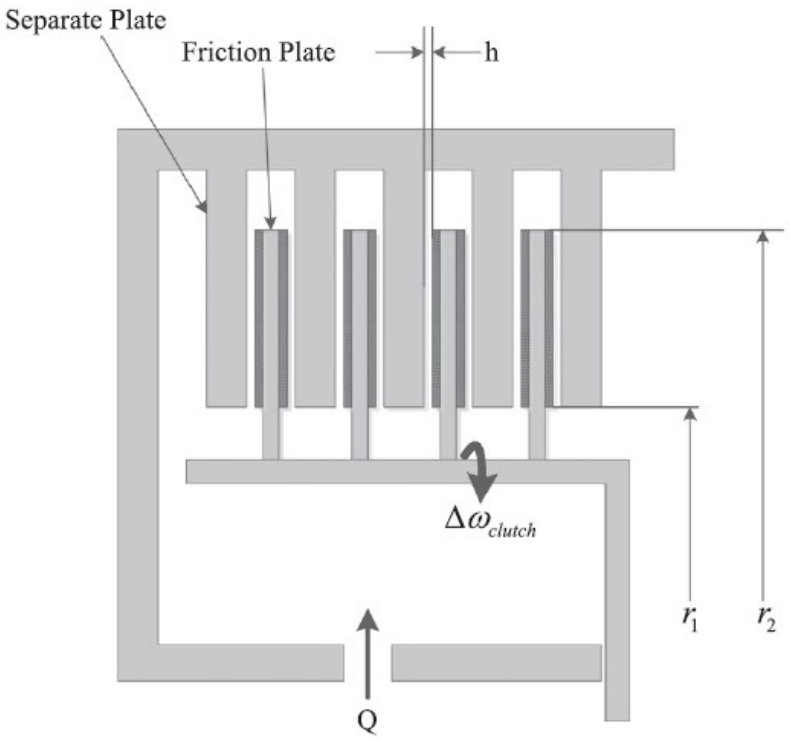

Figure 18 Schematics of opened clutch (15)

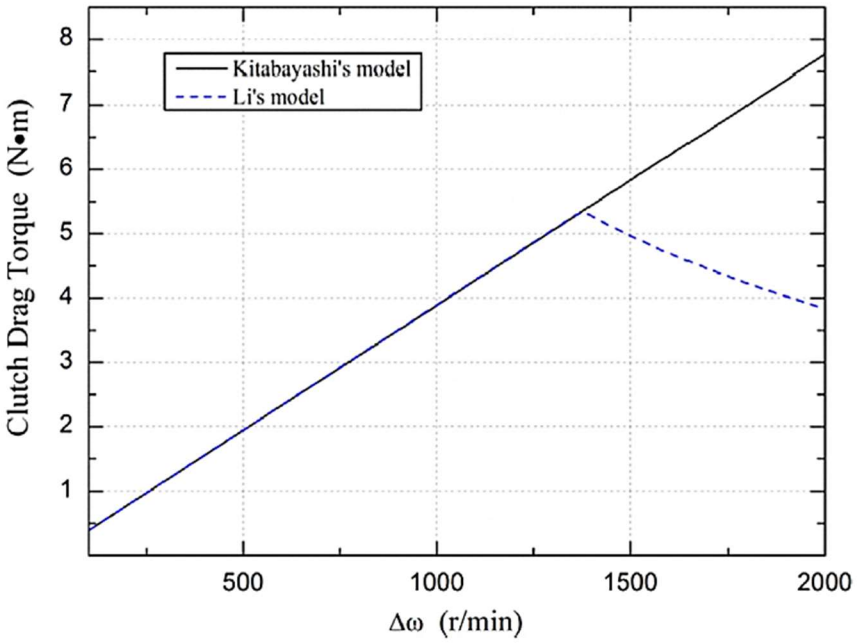

Figure 19 Kitabayashi's vs. Li's clutch drag torque model (15)

3.4 Design influence

As in conventional manual transmissions, also in dual clutch transmissions there are different flaws possible in the production and assembly of the whole transmission as well as of the different parts. Many of these flaws might lead to problems during synchronisation and rail control as their behaviour is not predictable sufficiently (2). In this thesis it was taken under assumption that every part of the system is produced and assembled ideally. Some of these flaws are listed and shown here:

- ***Proximity:***

  The axial alignment of the synchronizer ring and sliding sleeve chamfers (Figure 20) (2).

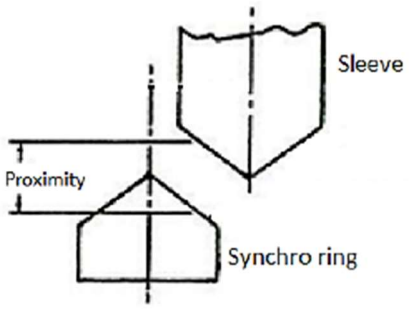

Figure 20 Proximity (2)

- ***Angle error***:

  Between the cone of the synchronizer ring and the gear synchronizer cone increased force may cause disengaging the gear into neutral (2).

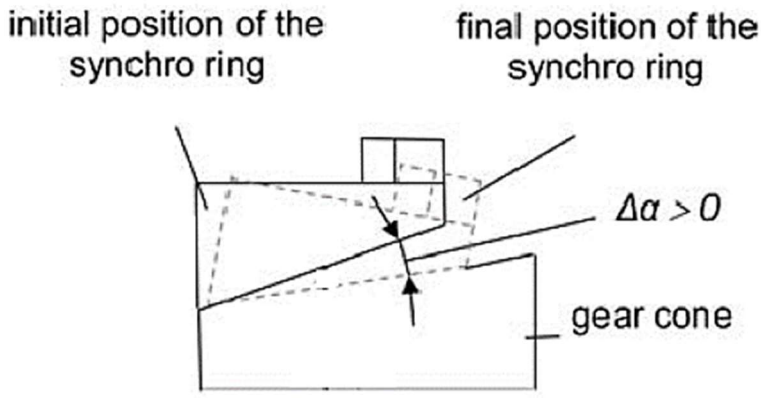

Figure 21 Cone angle error (2)

- ***Pitch error:***

  Relative position of more splines to each other where some of the splines are in contact with their right side chamfer and other with left side chamfer (Figure 22) (2).

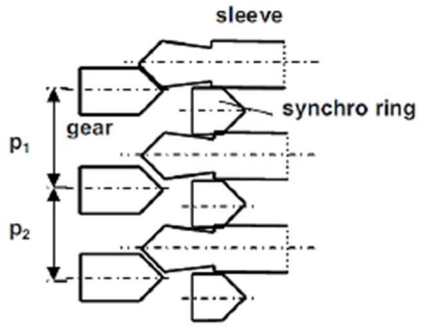

Figure 22 Pitch error (2)

- ***Position error***:

  This error occurs when not all splines between ring and the teeth are in contact during indexing (Figure 23) (2).

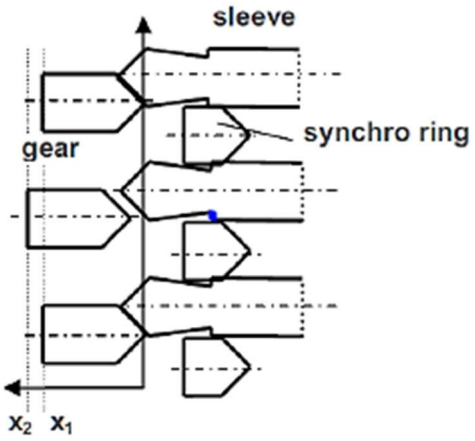

Figure 23 Position error (2)

- ***Cold gearbox***:

  Causes problems and stiff shifting due to the lower oil temperature especially in winter period. The force that is needed for the gear engagement must be higher to break the oil film in the cone and also between the chamfers (2).

- ***Fork Bending***:

  In Figure 24 the possible fork bending while force is applied is shown.

This can cause reduction of the shift force that is needed for synchronization (27).

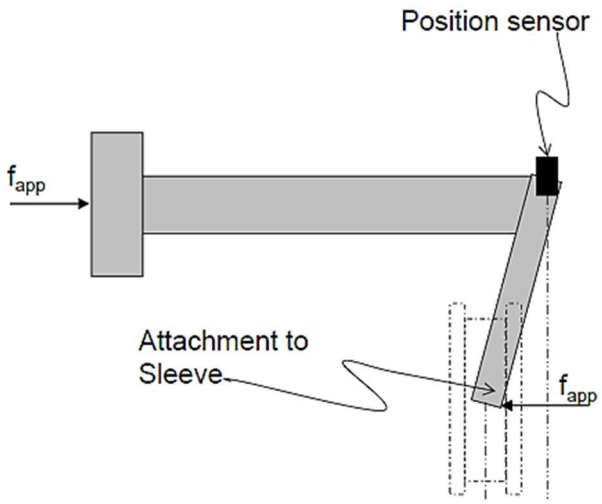

Figure 24 Fork (exaggerated) bending (27)

- **Stick-slip phenomena:**

  This phenomena was described in (2) as parameter that influences shift quality in manual transmission, but this phenomena is also one reason for the early ring unblocking, gear changing noise and cracking. It is influenced by the normal force and the sliding velocity of the contact surfaces, the sleeve side surface to the side of the ring splines, but more importantly also those in the cone friction surface. Figure 25 shows the principle of this phenomena. The simple sliding area is developed when the normal force on the friction surface is low and the sliding velocity is high. When the force increases and the velocity decreases, there are parts of harmonic oscillations and on the other hand where the force has its maximum, while the velocity is low, the stick-slip phenomenon might occur.

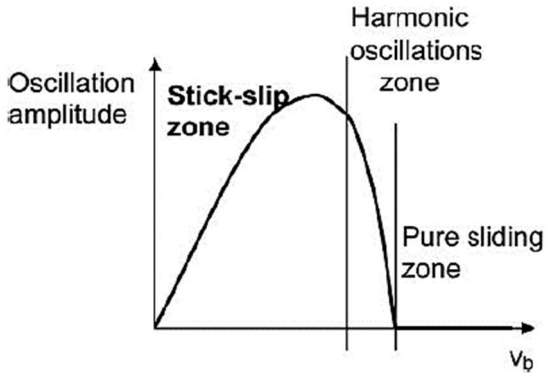

Figure 25 Stick-Slip phenomena (2)

4. Mathematical model

4.1 Overview

As it can be seen from previous chapter, different parts were involved in rail movement. In this chapter, previously discussed physics of rail movement is described with mathematical model. Figure 26 shows the approach for obtaining the mathematical model in this thesis. First, part interaction analysis has been conducted. Afterwards, free body diagrams and following equation of motions were obtained. With different simplifications, mathematical model has been concluded.

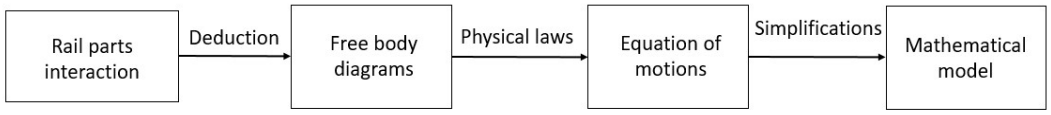

Figure 26 Mathematical model approach

As previously seen, there have been different phases of rail movement recognized. After the simplifications have been undertaken, the mathematical model was divided into different subsystems. Figure 27 shows five separately described mathematical subsystems, that were obtained through various simplifications. Each subsystem described different dynamics with different equation of motions. The simplifications have been described at the end of this chapter.

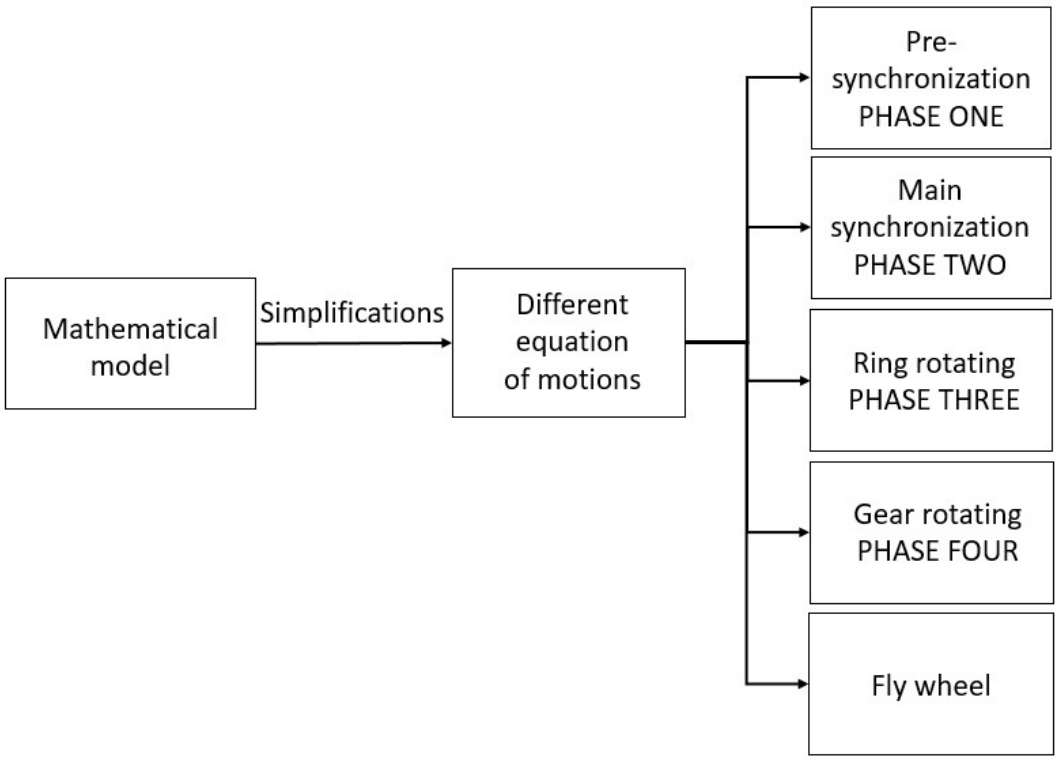

Figure 27 Mathematical model separation

4.2 Actuator and shift force

The authors of (23), (13), (25), (15) and other publications discuss the hydraulic actuation of the rail and describe the pressure applied on the actuating pistons. The pressure that is applied on the pistons is influenced by the net flow in the piston chamber. The author of (23) suggests that for the pressure actuation model, powertrain and vehicle models would be necessary. Because in this thesis the rail control model is designed as standalone model, the actuation of the gear preselection mechanism will not be further discussed, while the emphasis is made on the force level that is needed for the rail movement and gear preselection. As previously mentioned, the shift force is created through the pressure applied onto the pistons. Equation (4.1) represents the shift force, where *p* is pressure and *A* is the piston area. It is important to say that the pressure created by the hydraulic actuator is assumed to be equal to the pressure difference between left and right piston chamber.

$$F_{shift} = p * A \tag{4.1}$$

4.3 Synchronisation

4.3.1 Control model

Previously eight different synchronization phases were described and illustrated. In this chapter, a mathematical model of the synchronization phases is discussed and the equations of the motions for the modelling are presented. For the control model purposes, it is possible to describe the synchronization process within four main phases (15). Also the mathematical model of the free wheel phase has to be considered, whereby movement of the rail towards neutral and engagement position has to be described. It is considered that there is no distance between the strut detent face and the synchro ring and that just after the shift force has been increased, the strut detent face starts moving the synchronization ring. Even though there is relative rotation between the synchro ring and the sleeve, while the synchro ring gets into the blocking position, as the author of (2) suggests on page 27, it can be considered that the speed of the ring and the sleeve are equal, because the synchro body can be assumed as rigid body (23). Therefore, the hydraulic kinetic cone friction torque is created as soon as the shift force is high enough to start pushing the ball out of the sleeve groove and thus it can be described with rotational speed of the sleeve and the gear. The phase six, second fly wheel phase and also the phase eight, gear engagement, are not taken into account in the simulation model, due to achieve reduced calculation time and due to the small distance and short shifting time between start and end of both of these phases. Therefore, the ring rotation and fly wheeling phase are considered as one phase, where the emphasis is on the gear rotation behaviour. In addition, the indexing phase, gear rotation and gear engagement are considered as single phase. Finally, separate fly wheel phase is described and modelled, so that it is possible to simulate the movement of the sleeve in both directions, if the rail movement is aborted in certain position or moved toward the neutral position.

With these adjustments and simplifications of the synchronization process, the corresponding mathematical description was derived (15).

As the authors of (2) suggest, interaction analysis of the parts in the synchronizers for each phase would be necessary for the mathematical description. Strut detent vs. sliding sleeve, synchro hub vs. output shaft and strut detent vs. synchro hub are not represented in Table 1 as they are considered to be in constant contact with each other during the movement of the rail. The strut detent and synchro ring are in the contact during the whole synchronisation process. But after phase two is finished, the amount of load produced by strut detent onto the synchronisation ring is reduced to a minimum, whereby the amount of the load that holds the strut detent face in contact with the synchro ring is only produced due to the friction forces on top of the ball pin in the contact between the sleeve and the ball pin. Furthermore, in the phase three, synchronization phase, assumption is made that the sleeve is not moving toward the gear because it is blocked by the ring. Actually, that is not true, because due to the thermal expansion of the ring, the sleeve moves together with the ring slightly toward the gear as the ring diameter increases, but the sleeve is also unable to turn the ring until the speed is not synchronized. The thermal expansion model of the ring should be described in separate investigation, where the separate simulation model has to be developed for the diameter expansion. Nevertheless, for the simulation of the gear shift process in dual clutch transmissions, it is assumed that the gear preselection process can be modelled without the thermal expansion. Therefore, the sleeve is assumed to be in stationary position during the synchronisation phase.

Table 1 Interaction

PARTS	PHASE 1	PHASE 2	PHASE 3	PHASE 4
Synchro ring vs. Synchro hub	X			
Synchro ring vs. Gear		X	X	X
Strut detent vs Synchro ring	X	X	X	X
Synchro ring vs Sliding sleeve		X		

4.3.2 Definitions

Before coming to the mathematical model of the synchronization phases, for better understanding some of the forces, the torques and the equations of the motions are defined in this section and also shown by use of free body diagrams.

- ***BTL or Break Through Load*** – This load is the first resistance force against the movement of the sleeve from neutral position. This force is produced through the spring and ball under the sliding sleeve. Equation (4.2) shows the mathematical expression of the connection between the shift force and the spring force under the sliding sleeve, while Equation (4.3) represents the load, where n_p stands for number of the strut detents in the synchro hub. Figure 28 shows the free body diagram of the ball pin and the groove of the sleeve. With the equilibrium equations, derived from this free body diagram, the break through load is calculated. Force with blue arrows in this diagram stands for friction force in the

contact point between ball and the groove of the sleeve. Force with green arrows stands for normal force on the surfaces in this contact point. The value of this load changes with the movement of the sleeve as the ball moves out of the strut and presses the spring, while changing the spring force. There is also a geometrical constraint for the movement of the spring, that is described by Equations (4.4) and (4.5). In these equations the connection between the sleeve displacement, detent movement and the vertical spring movement and length of the spring with the spring force is described. The equation for the spring force also considers bending of the spring. In Figure 29 different types of strut detents are shown. As it can be seen, the different geometrical design of the strut detent influences the mathematical equation accordingly. Therefore, the equations that are presented here are only valid for the ball type. For the other types, the equations differ according to the geometry characteristics (2).

$$F_{BTL1} = F_{spring} * \frac{\mu_{sl}+tan\theta}{1+\mu_{sl}*tan\theta} \tag{4.2}$$

$$F_{BTL} = F_{BTL1} * n_p \tag{4.3}$$

$$F_{spring} = k_{spring}(L_{spring,0} - \sqrt{{x_{sd}}^2 + {L_{spring}}^2}) \tag{4.4}$$

$$x_{sl} - x_{sd} = \frac{\Delta y_{sd}}{\tan\theta} \tag{4.5}$$

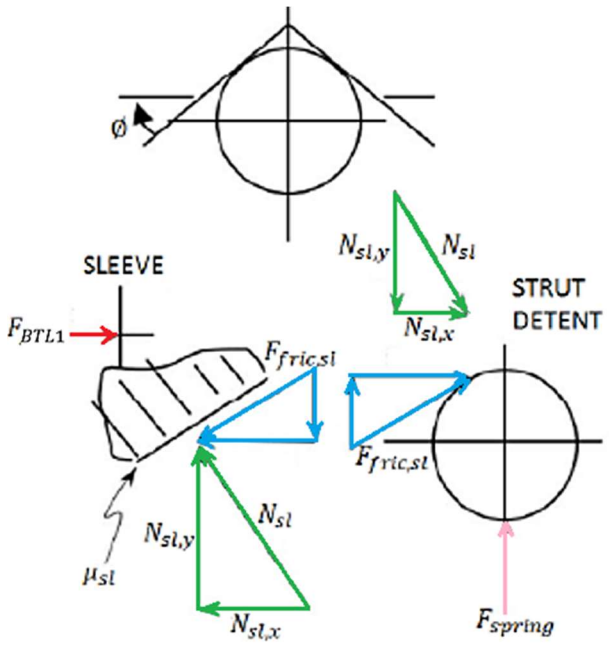

Figure 28 BTL-Strut detent (2)

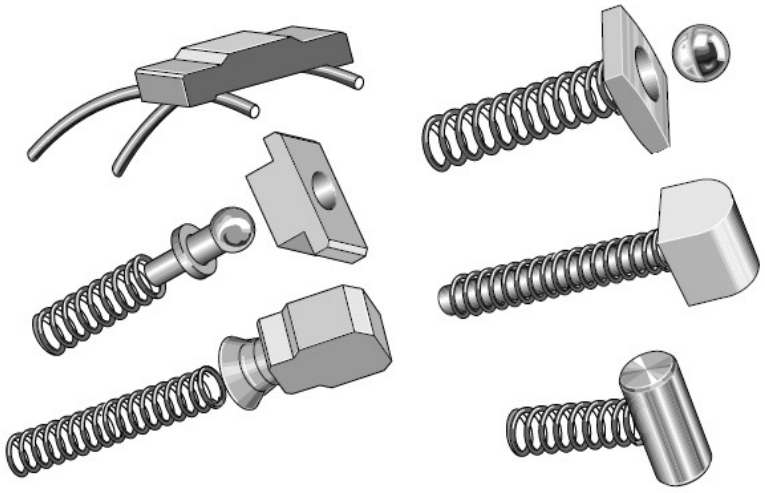

Figure 29 Strut detent design (22)

- ***Cone friction torque*** – also known as synchronization torque - is generated due to the friction between the synchronization ring inner cone and the gear synchronization outer cone. Figure 31 shows the contact between ring cone and gear cone. The forces that are represented here are part of the ring cone free body diagram, where the force with green stand for normal force on the cone surface and the force with yellow stands for the frictional force in the cone. Force with red arrow stands for shift force transferred through the fork and the sleeve. With Equation (4.6), (4.7), (4.9), and (4.10) that give the mathematical definition of the forces from the free body diagram and the connection with the torque, it is possible to derive the main speed synchronisation cone friction torque. The mathematical representation of the cone friction torque is shown in Equation (4.8). As discussed, for each phase there is different cone friction torque applied on the gear cone. In this equation, first torque is created due to the hydraulic film in phase two as described from author of (23) on page 324, where h stands for thickness of the film and μ for the oil viscosity. The second torque is the main speed synchronisation friction cone torque in phase three. The third torque describes the static torque in the cone after the speed synchronisation in phase four, phase five and phase six, while the last torque shown here is the torque produced after the ring has been separated from the gear. But due to the side friction between the chamfers in the sleeve teeth and the gear teeth, there is still a small amount of friction torque in the cone. It is important to note that the cone friction coefficient is nonlinear and described by the authors of (28) on page 94 with the Stribeck curve shown in Figure 30, where three different phases of lubrication and further coefficients of frictions are shown. The authors of (28) and (2) described the mathematical model for each region of this curve (28), (22), (2), (23).

$$N_C = F_{fork} \frac{1}{\sin \alpha_c} \tag{4.6}$$

$$T_C = F_R N_C \tag{4.7}$$

$$T_C = \begin{cases} K_{CC} 4\pi\mu {R_C}^3 b \frac{\dot{x_{sl}}}{h}\left(1 - \frac{\omega_{tg}}{\omega_{sl}}\right) \\ \frac{\mu_c F_{fork} R_C}{\sin\alpha_c} \\ T_{Cstatic} \\ \frac{\mu_c F_{fric\_s} R_C}{\sin\alpha_c} \end{cases} \tag{4.8}$$

$$K_{CC} = 1 + (1 - n)\frac{a}{b_i} \tag{4.9}$$

$$b_i = b - n\frac{a}{2} \tag{4.10}$$

$$\mu_c = \mu_{solid} + \frac{\mu_{solid} - \mu_v}{S_2 - S_1} S_1 - \frac{\mu_{solid} - \mu_v}{S_2 - S_1} \cdot \frac{\mu(\omega_{tg} - \omega_{sl}) R_c}{F_{fork}} 4\pi R_c b sin\alpha_c \tag{4.11}$$

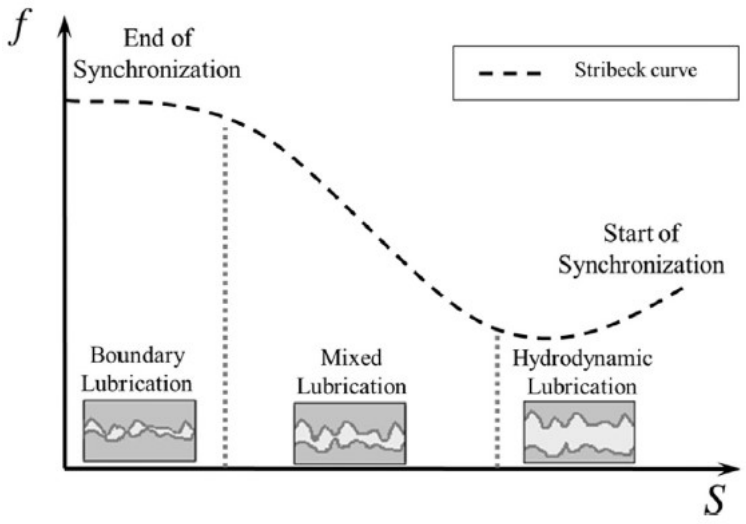

Figure 30 Stribeck curve (28)

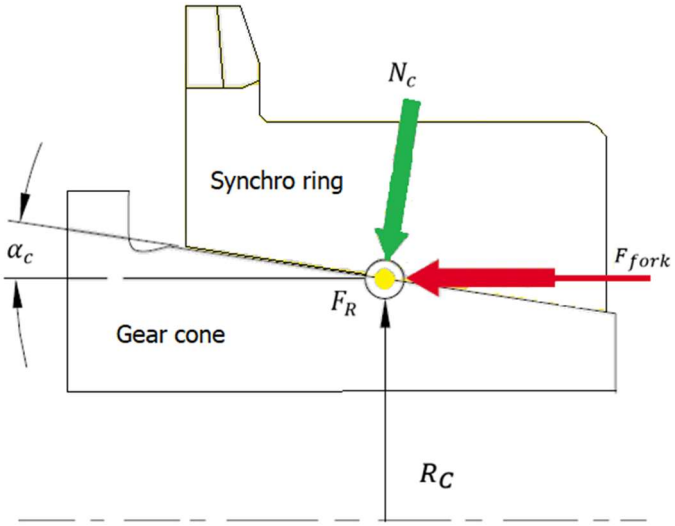

Figure 31 Friction cone (22)

- ***Blocking and indexing torque*** – In Figure 32, the free body diagram of the sliding sleeve chamfers with the synchro ring chamfers is shown. With the help of this free body diagram, the mathematical definition of the indexing or blocking torque is obtainable. Force with green arrows stands for the normal force on the chamfer surface in the contact point, while the force with blue arrow stands for friction force in the surface contact point. For the indexing torque there is a possibility that the chamfer angle is different, but in this thesis, all chamfer angles are assumed to be equal. The indexing or blocking torques can be derived by mechanical laws based on the free body diagrams from Figure 32 and Figure 33. In Figure 33, tangential force (red arrow) that creates this torque is derived from the components of friction and normal sleeve force on the chamfers shown in Figure 32. Derivation of the indexing torque is well known. Exemplary, the authors of (22) on page 22 show the complete derivation steps that are explained here. Equation (4.12) shows the mathematical representation of this torque (2), (22). With the forces in the contact between the chamfers shown in the free body diagram, the connection between normal force and friction force with friction coefficient can be calculated. Furthermore, these two forces can be expressed by shift force and also by the indexing torque at the output shaft radius. Assuming that the chamfer angle of the ring splines and gear synchronization splines are equal, the only difference between the indexing and the blocking torque is characterized by the side friction forces (yellow and red arrows) between the ring splines and sleeve splines as it can be seen in Figure 34 (2).

$$T_I = F_{fork} R_{sl} \frac{1-\mu_{ch} \tan \beta}{\mu_{ch}+\tan \beta} \tag{4.12}$$

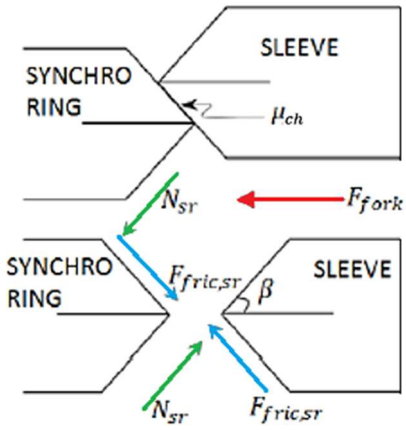

Figure 32 Blocking torque perspective 1 (2)

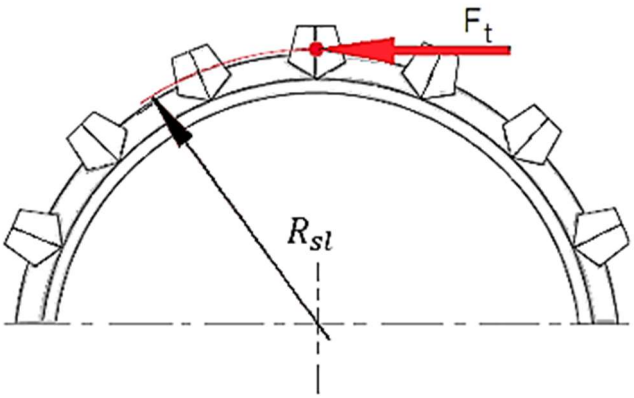

Figure 33 Blocking/Indexing torque perspective 2 (22)

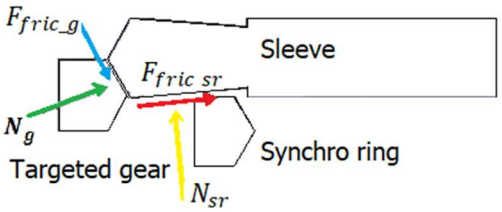

Figure 34 Indexing torque (2)

- ***Geometry*** – In Figure 35 and Figure 36 all geometry parameters that are necessary for the mathematical model are illustrated. In these figures the body number one represents the targeted gear, where number two represents the synchronizer ring. Other important dimensions are the cone angle and the number of cones, possible shift distance s and the distance b_0 between the gears where the chosen synchronizer acts. These figures also show the mean cone diameter d, where the normal force acts on the cone and the largest cone diameter d_0 with teeth interlock diameter d_C.

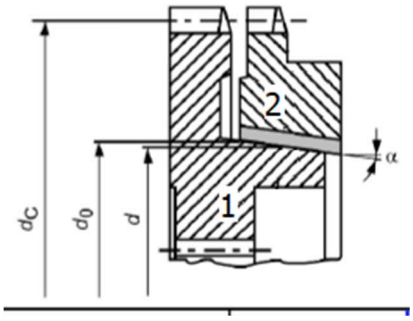

Figure 35 Single-Cone synchronizer body geometry (21)

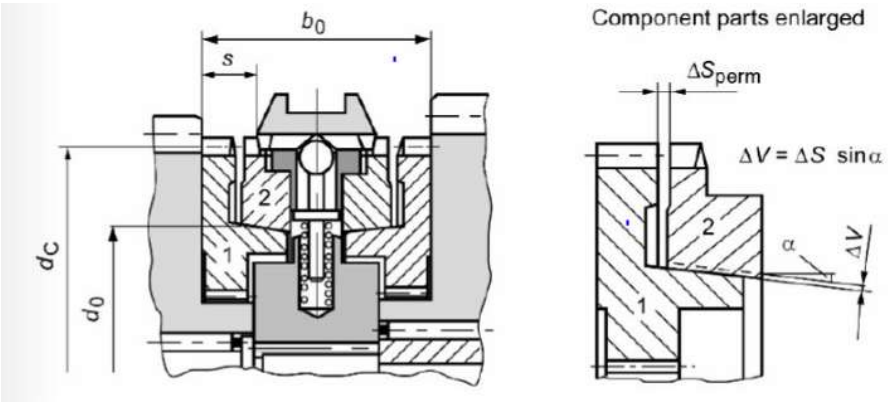

Figure 36 Assembly synchronizer body geometry

- ***Sleeve rotational speed ω_{sl}*** – For simulation of the gear shift process of dual clutch transmission, different motor torques are predefined by the actual driving conditions. The sleeve rotational speed is calculated from the current driving conditions and can be derived through current rotational speed of the closed clutch and the current gear ratio. Because in DCT there are two input shafts, which are connected by two clutches and two output shafts that have equal output shaft gears connected together by one input gear for the differential shaft (11). Another possibility to calculate the sleeve speed is based on the output shaft speed, differential ratio and the input gear ratio of the differential shaft. Equation (4.13) presents the sleeve speed derived from the closed clutch speed, which is used in the model. Due to the inertia torque of the vehicle, assumption is made that the rotational speed of the sleeve is approximately unaffected by the synchronisation process, because the inertia of the targeted gear is significantly smaller than the total inertia that is reduced by the sleeve as the sleeve is rigidly connected with the output shaft. For estimation of the rotational speed of the ring and the strut detent it is also possible to assume that it is the same as those of the sleeve, because it can be assumed that the synchronizer body is a rigid body (2), (23), (29).

$$\omega_{sl} = \frac{\omega_{cc}}{i_{cg}} \tag{4.13}$$

4.3.3 Phase one

For each phase the mathematical model is described by equations of motion of the targeted gear and the axial movement of the rail. At the beginning of phase one it is considered that the distance between the first contact of the strut detent face to the synchro ring is approximately zero so that after increase of the shift force the strut detent will push the ring towards the gear. Figure 37 includes an illustrative representation of the forces and torques that influence the phase one, whereby red splines represent the gear splines, blue splines illustrate sleeve splines and yellow splines the ring. The length of the vectors shown in this figure also show, which forces or torques are mostly influencing the sleeve movement or the gear rotational speed. This illustration shows the synchronization ring with the forces that are applied on it through the interaction between the face of the strut detent and the tangential and radial friction forces on the synchronization ring cone, through the contact with the gear cone. The mathematical equations that represent the axial movement of the sleeve and the fork are represented in Equation (4.14) and in Equation (4.15) the motion of the targeted gear is represented. In this mathematical description, the forces that resist the axial sleeve movement are friction forces due to the movement of the sleeve and the break through load. The gear rotational speed is influenced by the hydraulic kinetic cone friction torque, drag clutch torque and other drag torques, while the corresponding gear ratio of the targeted gear has been taken into consideration. The sign function in the equation describes if there is a downshift or upshift engagement process, while comparing the sleeve and the gear speed (15). Furthermore, the moment of inertia for the equation of the motion of the targeted gear is reduced a moment of inertia that considers the moment of inertia of the opened clutch, input shaft and all other rotating gears that are connected to this shaft. This can be calculated with Equation (4.16).

$$(m_f + m_{sl})\ddot{x}_{sl} = F_{fork} - F_{fric} - F_{BTL} - F_{slr} \tag{4.14}$$

$$J_{geari}\dot{\omega}_{tg} = sign\,(\omega_{sl} - \omega_{sl})\,K_{CC}4\pi\mu {R_C}^3 b\frac{\dot{x_{sl}}}{h}(1 - \frac{\omega_{tg}}{\omega_{sl}}) + sign\,(\omega_{sl}i_{cg} - \omega_{tg}i_{tg})T_{cd}i_{tg}i_{tg} + T_d \tag{4.15}$$

$$J_{geari} = J_{geari} + \frac{J_{red}}{i_{tg}^2} \tag{4.16}$$

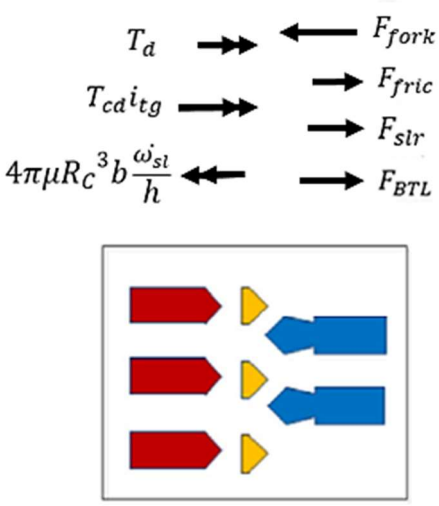

Figure 37 First phase (15)

4.3.4 Phase two

The main part of speed synchronisation occurs in phase two. This phase can be described by Equation (4.17) under the assumption that there is no movement of the sleeve due to ring blocking, while it is assumed that the strut detent has travelled its maximal vertical distance. It is also assumed that the strut detent and ring have reached their maximal axial position. Therefore, the second phase is described by speed synchronisation by Equation (4.18) and illustrated in Figure 38, where the cone friction torque either slows or accelerates the gear, which is expressed by use of the sign function. Accordingly, the clutch drag torque under consideration of the gear ratio of the targeted gear either supports this process or resists it, which is also expressed by the sign function. During this process Equations (4.19) and (4.20) have to be fulfilled. Here the clutch drag torque has to be always larger than the resisting drag torques in first equation and in second equation larger than the indexing torque on the chamfers between the ring and the sleeve, so that it does not come to an early ring unblocking before the speed has been synchronized. As the author of (25) on page 13 explains, this can occur when oil whipping at the cone surface in phase one is insufficient, which may lead to a lower friction coefficient. The blocking safety factor in Equation (4.20) is a design parameter, which is assumed that it is always is true in this thesis. In addition, it is assumed that the sleeve cannot move forward until the speed has not been synchronized (15).

$$\left(m_f + m_{sl}\right)\ddot{x}_{sl} = 0 \tag{4.17}$$

$$J_{gear1}\dot{\omega}_{tg} = sign\left(\omega_{sl} - \omega_{sl}\right)T_c + sign\left(\omega_{sl}i_{cg} - \omega_{tg}i_{tg}\right)T_{cd}i_{tg} + T_d \tag{4.18}$$

$$T_c > \left(T_{cd}i_{tg} + T_d\right) \tag{4.19}$$

$$T_c > T_I \tag{4.20}$$

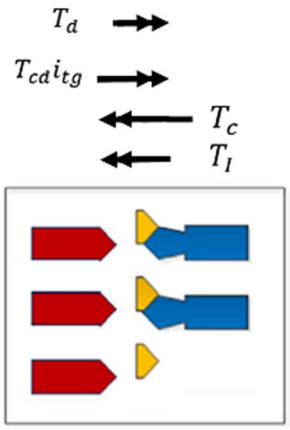

Figure 38 Phase 2 (15)

4.3.5 Phase three

In phase three after the gears are synchronised, the sleeve turns the gear and the ring together in order to move axially, according to the works (2), (23), (30). On the other side different manufactures of the synchronizers mention in different works, e.g. (20), (22), that only backward rotation of the ring takes place in this phase, while the gear will not be affected during this rotation process. Here it is discussed the Equations describing the rotation of the gear and the ring together, while for the control modelling only the ring rotation is modelled. After the speed is synchronized, the ring is stuck on the gear cone with the static friction torque that holds this connection together. This static friction torque can be described by the pressure in the cone and the static friction coefficient. This torque will not be considered in this phase and it will be assumed that during gear rotation phase it does not influence the dynamics. In Figure 39 the illustration of phase three is shown, where the indexing torque has to be larger than the total resistance drag torque so that the ring rotation is possible. Also here are all friction forces shown, that are a result of the contact between sleeve and all other parts during the sleeve movement. This friction can also be neglected as it is really small compared to the sleeve acceleration and the total drag torque. Equation (4.21) shows the ring and gear rotation due to the indexing torque on the ring splines. Also, Equation (4.22) shows the connection between gear rotation and axial movement of the sleeve through the ring unblocking phase. These equations show that the sleeve movement is only possible if the condition in the Equation (4.23) is satisfied (15). The difference between ring rotation alone and the rotation of the gear and the ring together is different moment of inertia that has to be turned, as well as the clutch drag torque. For the modelling of this phase, only the rotation of the ring has been considered, while the gear speed has been considered to be unaffected with this rotation. Also the authors of (29) made experimental measurements of the synchronization process, where it can be seen that the gear speed and the sleeve speed during the phase three stay synchronized.

$$(J_{geari} + J_{sr})\dot{\omega}_{tg} = sign\left(\omega_{sl}i_{cg} - \omega_{tg}i_{tg}\right)(-T_I + T_{cd}i_{tg}) + T_d \qquad (4.21)$$

$$\dot{\omega}_{tg} = \frac{\ddot{x}_{sl} \tan\beta}{R_{sl}} \tag{4.22}$$

$$T_I > (T_{cd} i_{tg} + T_d) \tag{4.23}$$

$$(m_f + m_{sl})\ddot{x}_{sl} = F_{fork} - N_{sr}(sin\beta + \mu_{sl} cos\beta) - F_{fric} \tag{4.24}$$

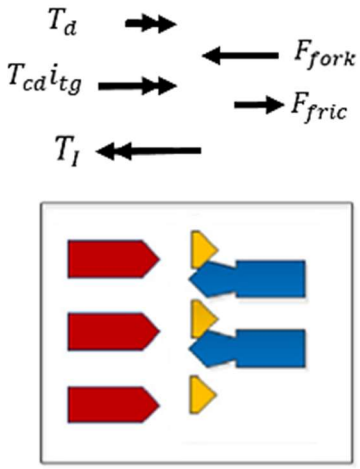

Figure 39 Ring unblocking (15)

4.3.6 Phase four

In the final phase, during the indexing, there are couple of possibilities for the sleeve alignment as earlier mentioned. Therefore, one random variable was implemented into the equation of the motion for the last phase, that will represent the alignment of the gear teeth and the sliding sleeve teeth. This was introduced by (15) in the Equation (4.25) with the random variable z, which describes the relative position of the sleeve spline and the gear spline. This variable returns a value with uniform probability from an interval $(-\frac{p}{2}, \frac{p}{2})$ where p is the pitch of the gear splines. Figure 41 shows the different possibilities at indexing phase, with both downshift and upshift scenarios shown. The worst case scenario in this process is when two splines get in the contact with the tops of the splines, where theoretically engagement will be impossible, but as the author of (31) suggests that in the reality, due to the vibration, oil and dynamics the splines will always be able to slide on both sides of the chamfer. The Equation (4.26) shows the connection between the gear acceleration and sleeve speed, where the random value explained earlier affects the angular acceleration accordingly (2).

The indexing phase is shown in Figure 40, where the same forces and torques are describing this phase as it was in the previous one but here the different equation of the motion is introduced. In this phase just before the indexing of the splines occurs, the static friction that was holding the gear and sleeve spinning with the same speed will be broken and the ring will be separated from the gear. In this case if the force after the separation for the axial movement and the indexing torque is not high enough to ensure that indexing torque will be greater than the drag torque, possible blocking or noise issues can occur. Therefore, it is also important that in this phase indexing torque is greater than the total

resistant drag torque. After the ring has been separated from the gear, in the cone between the gear and the ring, there will be a certain amount of the cone friction torque presented. Because in DCT the gear preselection occurs while other shaft is closed and driven, the drag torque in the clutches can also help the rotation of the gear, where after the separation of the ring and the gear, desynchronization will be reintroduced. The gear slipping in this case can be described, with equation (4.18), where only side friction from the contact between splines of the sleeve and the ring splines and on the other hand the contact of the sleeve with the strut detent create the friction torque in the cone (25). Also the axial movement can be described with the Equation (4.27), where the normal force is shown in the previous chapter, where indexing torque has been described (2).

$$J_{geari}\dot{\omega}_{tg} = sign\,(z)T_I + sign\left(\omega_{sl}i_{cg} - \omega_{tg}i_{tg}\right)T_{cd}i_{tg} + T_d \tag{4.25}$$

$$\dot{\omega}_{tg} = 2\frac{\dot{x}^2_{sl}\,\tan^2\beta}{R_{sl}z} \tag{4.26}$$

$$\left(m_f + m_{sl}\right)\ddot{x}_{sl} = F_{fork} - N_g(sin\beta + \mu_{sl}cos\beta) - F_{fric} \tag{4.27}$$

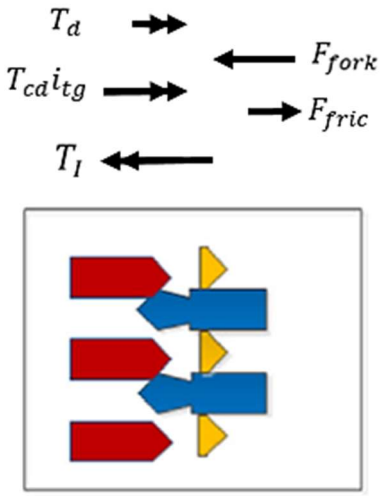

Figure 40 Indexing torque in the last phase (15)

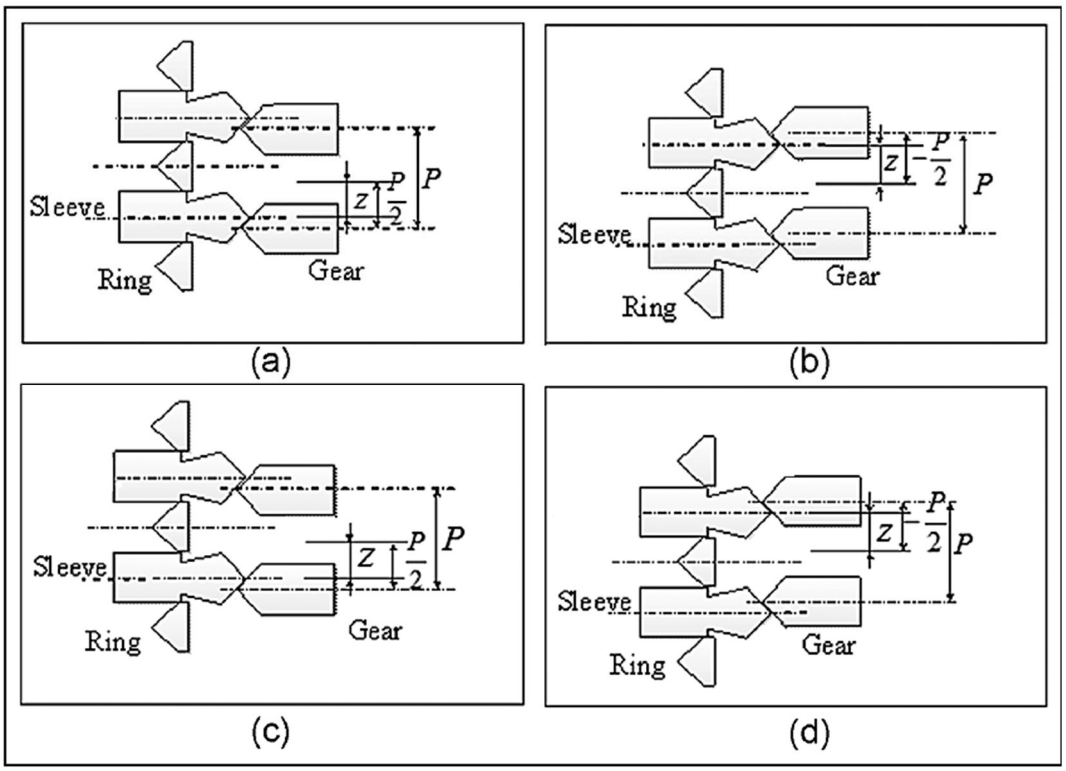

Figure 41 Random alignment a) upshift z>0; b) upshift z<0; c) downshift z>0; d) downshift z<0 (29)

4.3.7 Fly Wheel

As described above for the simulation purposes, the fly wheel phase has been also considered. The Equation (4.28) describes the axial movement of this phase. This equation also describes the movement to the neutral position. Various authors also described that in this phase, the static friction in the cone between ring and the gear, that is holding the ring and the gear stuck, can be lower than the drag torque. This further causes the desynchronization between the gear and the sleeve. In this thesis, for the Simulink model, it is assumed that in this phase there is not any desynchronization in this phase and that the gear speed and the sleeve speed remain equal.

$$(m_f + m_{sl})\ddot{x}_{sl} = F_{fork} - F_{fric} \tag{4.28}$$

4.4 Clutch Drag Torque

Previously the influence of the clutch drag torque on the synchronization have been discussed and described which losses are producing the drag torque. In this section the mathematical descriptions of these losses will be considered, where the emphasis of these losses are made on the losses caused by clutch drag torque. As the author of (32) explains, there are some uncertainties about these mathematical models that are here represented, as for some of them full CFD simulation has to be undertaken, which due to the small influence of some of these losses to the synchronization process was excluded. For the modelling of the drag torque, only clutch drag torque will be taken into the consideration, because it has been identified as the main cause for synchronization failure

whereby the other losses are mainly influencing the gear shift quality in manual transmission, which is mainly described as the needed input shift force from the driver and the double bump effect (2), (32).

1. Load dependent bearing losses (32):

$$C_L = f_L F d_m \tag{4.29}$$

2. Tooth friction losses (32):

$$P_M = \frac{f\ T\ N\ cos^2\beta}{9549\ M} \tag{4.30}$$

3. Concentric shaft shear (32):

$$T = 4\pi\mu h \frac{(r_2^2 r_1^2)}{(r_2^2 - r_1^2)}\omega \tag{4.31}$$

The main part of drag torque is caused by clutch shear losses, also called clutch drag torque. Due to the lots of uncertainty about the clutch drag torque, it is not possible to measure it clearly. Different approximate models were developed where we already mentioned some of them in chapter Rail-physics. In this section the Equation (4.32) represents the mathematical model of the Liu's approximation, where the main parameters for this model are number of friction plates N, the friction coefficient of these plates, effective radius of oil film, inner radius of clutch plate, distance between plates and relative rotation speed between different clutch pairs where the rotation speed of closed clutch and rotation speed of open clutch are mainly affected by the dynamic viscosity. As it is explained in (29), for the calculation of the effective radius of oil film in clutches, the actual flow rate through clearance of the clutch is required to be compared with the flow rate that is required to maintain a full oil film. This is necessary because in the high rotational speed the drag torque is not linear with the speed difference of the clutches. It is also important to note, that the drag torque always tries to slow down the rotating components. Therefore, this torque assists the cone drag torque during the deceleration of the gear and resist during acceleration (2).

$$T_{cd} = \frac{N\pi\mu_{cd}(r_e^4 - r_1^4)}{2h}|\omega_{cc} - \omega_{oc}| \tag{4.32}$$

4.5 Furthers simplifications

For some forces and other values that were described in mathematical models, simplifications were undertaken as the obtaining of the gearbox parameters are often incomplete to find for the modelling of a single existing dual clutch transmission. Also the author of (23) on page 323 suggests that given the approximate duration of

synchronization lasts 100 [ms] and that the inertial of the target gear is significantly smaller than the one of the vehicle, it is possible to assume the synchronizer model as rigid body. As the authors of the (15) described, where do certain phases end and start is not easily recognizable, therefore, these distances are only obtainable through the calibration process and for the simulation purposes of this model, these values were exemplarity. Other simplifications are enlisted here:

- The thickness of the film for the hydraulic torque is considered as linear dependency of the sleeve position, with initial thickness as the sleeve is in neutral position
- Further, for the drag torque model at high speed, there is not any know fluid flow rate in the clutch pack, as this model was purely standalone model made for further investigation of the gear preselection strategy and gear shifting in dual clutch transmission. Therefore, for the simulation purposes the clutch drag torque was calculated with the simplified model from the author of (15) which neglected the effect of the oil film shrinking and assumed that full oil film is maintained for every operating point. The Equation (4.33) shows the mathematical model for the drag torque that was used for Simulink modelling

$$T_{cd} = \frac{N\pi\mu_{cd}(r_2^2 - r_1^2)r_m^2}{h}|\omega_{cc} - \omega_{oc}| \tag{4.33}$$

  Also other drag torque caused by the bearing, oil etc. were neglected.
- The driving conditions that were implemented into this model, opened and closed clutch speed, were taken as example and do not correspond to the real timetable for the gear preselection.
- *Figure* 42 shows the schematics of the simplified physical model of the rail model, as the losses of the output shaft to the wheels are not included and the current speed of the sleeve is not affected through the synchronisation process.
- The influence of the temperature in the gearbox has not been included into the consideration, it has been taken under assumption that the preselection process takes places under the working temperature of the gearbox.
- Because of the fact that approximate duration of the gear preselection process is under the 200 [ms], it is considered that the gear synchronisation takes place during constant driving conditions.
- The break through load has been simplified so that spring force was only dependable on the sleeve position and the spring length change has been described with linear dependency of sleeve displacement, where the maximum length was at sleeve in initial position and the minimum length at the end of phase one, where the minimum length is approximately the interlock radius and maximum the groove radius.
- Possible oil damping effect during rail movement is also neglected
- For the indexing torque, the side friction forces that reduce the indexing torque were neglected

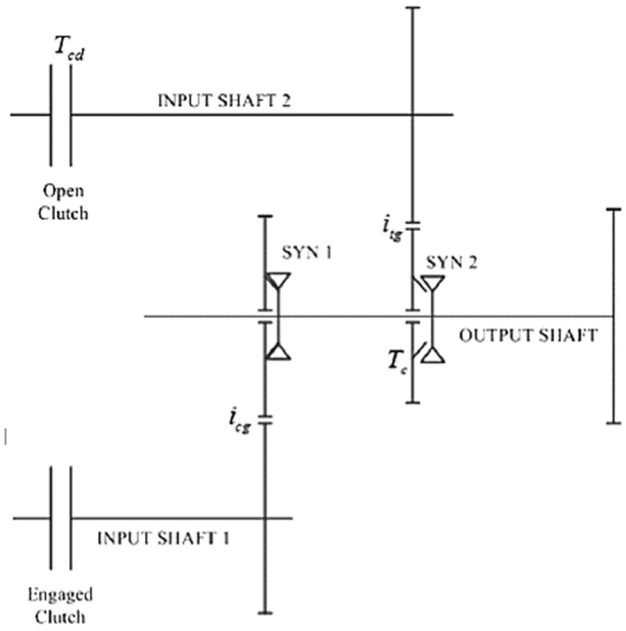

Figure 42 Simplified structure for the model (15)

5. Simulink model

5.1 MATLAB Simulink

Simulation model was built in MATLAB Simulink. MATLAB Simulink, a program developed by the company Mathworks, is a Model-Based Design in block diagram environment, that supports numeric simulation using different solvers, continuous testing and code generation as written in (33). Even though in the MATLAB Simulink environment there are many toolboxes for different types of systems, it was agreed that this model is only going to be built by using standard MATLAB Simulink toolbox with only low level components such as gains, integrator etc. The MATLAB Simulink model is also shown in appendix section of this thesis, while the other parts of the model are described and illustrated in the following sections. MATLAB version R2017a was used for this thesis.

5.2 Architecture and plant model

After the mathematical model has been obtained, the plant control model of the rail with different subsystems that calculates the four main phases described above, as well as the fly wheel phase for both sleeve directions has been developed. Modelling approach is shown in Figure 43.

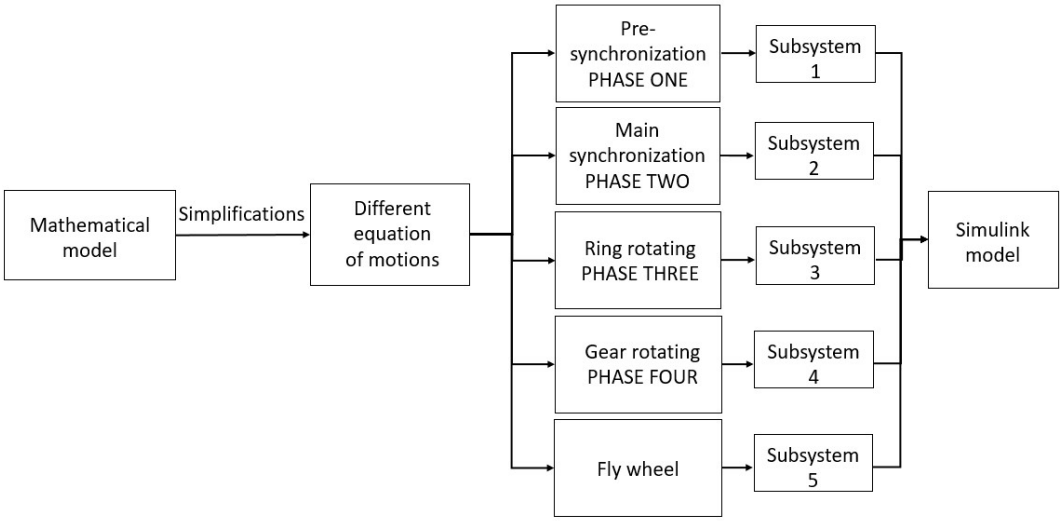

Figure 43 Modelling approach

Each of those subsystems calculate the gear speed through the synchronization process according to the equations of motion and also the sliding sleeve position, while different inputs from the actuator and from the signal builder are needed. The following

inputs are needed from the signal builders for the plant model block as initial and boundary conditions:

- Current driving condition:
  current speed of the closed clutch with current gear and the current speed of the opened clutch.
- Current position of the chosen rail.
- Targeted gear

Furthermore, shift force as main input is necessary for the calculation of the rail position and for the gear speed. Figure 44 illustrates signal flow of the model and the rail position calculation. Here the control block is also illustrated, which needs different input signals. From signal builders targeted gear and current driving conditions are needed. Feedback signal from the model block with calculated rail position and gear and sleeve rotational speed is also necessary for controller block. The output from the controller is the signal that represents the current that flows to the actuator block, which is then transferred accordingly to the shift force. As earlier mentioned, the emphasis in this thesis is the force level for the actuation of the rail, therefore the actuator block models simple actuator. More about this simple actuator will be explained later.

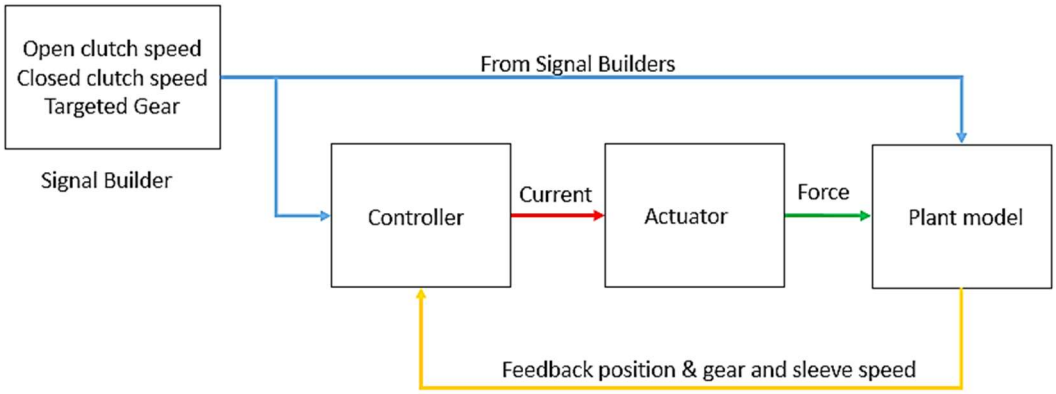

Figure 44 Simulink architecture

In the plant model block each of the phases described in the mathematical model have been modelled within the enabled subsystems. In the plant model the opened clutch and closed clutch speed are recalculated into the sleeve and targeted gear speed for the initial conditions. Each phase of the plant model is enabled only if certain rail position is reached. The rail position calculation within these phases is saturated only to output the highest possible position that corresponds the end or the start position of the current phase.

Triggers for each phase were implemented with state machine within the plant model block. The state machine is implemented with Stateflow block into the Simulink plant model block. Stateflow is used here as sequential decision logic based on state machines and flow charts (34). Because of the different phases being calculated and because this is continuous model, it was necessary to implement one Stateflow block. With the Stateflow chart, states were changed while different triggers were output for the corresponding enabled subsystem, whereby the switching condition for the single

events were reaching different shift rail positions or reaching the same rotational speed between the targeted gear and the sleeve.

In Figure 45 the logic behind the state changing is shown. From this scheme it can be seen that the rail position calculation and the synchronization of the gear and the sleeve speed can only be initiated as soon as the force is greater than zero. As soon as the force is greater than zero, first state is started while the output from this state is a trigger for the calculation of the sleeve position and gear speed using the equations from phase one. After reaching certain axial position, in this case the geometrical position that will mean that the sliding sleeve chamfer and blocking ring chamfer are in contact, the state two is switched, where the corresponding trigger is sent to the model, so that the equations of the phase two can be calculated. As long as the speed is not synchronized this state has not been changed, and after the absolute speed difference is lower or equal to some small (predefined) value, the state and the trigger are changed so that the equations from the phase three can be calculated. Again, here, the state is not changed until certain position is reached.

For the fly wheel phase after the gear rotation, switching condition is implemented directly into the subsystem for the phase three. It is assumed that the ring is turned after the sleeve has reached the position where the chamfers are no longer in contact. By reaching the certain position where contact between the tips of the sleeve splines and gear synchronization splines is expected, next state is reached and new trigger for the calculation of the equations of the phase 4 is created. The end condition for this state is also reaching said position, which means that the gear is engaged.

Furthermore, there is another state in the Stateflow chart for the movement of the rail to the neutral position, wherein the switch for this state is negative force, which corresponds to the pressure applied on the piston on the other side of the rail. It is possible to reach this state from every other state during the calculation of the rail movement. It is also possible to go to the neutral position if the other gear is currently engaged, which is not shown here for better overview of the Stateflow logic. As it can be seen, from this state it is again possible to go into any of the previously described phases,

while the switching conditions are the force direction change and the current position calculated from the axial movement within the neutral state.

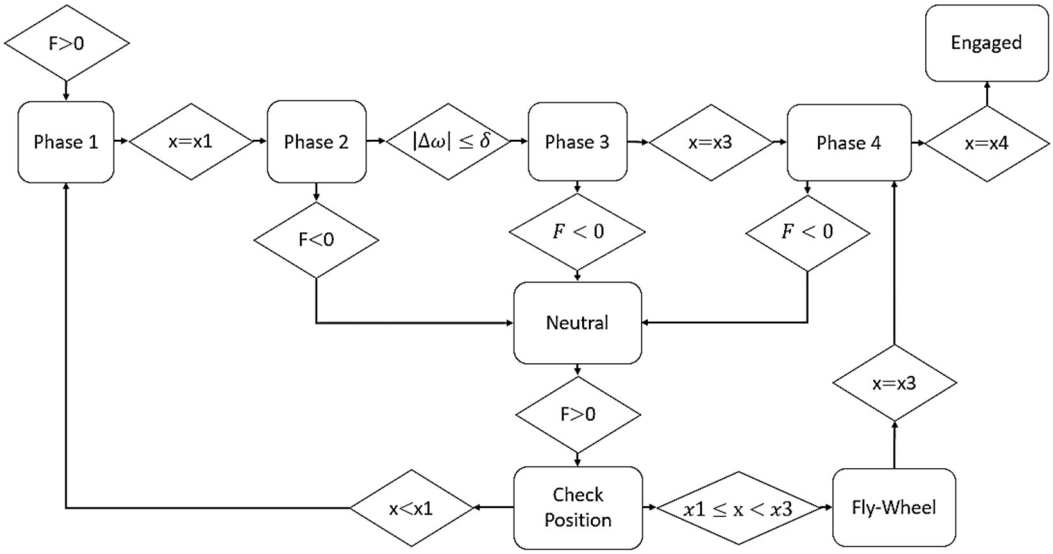

Figure 45 State-Machine for the each phase

5.3 Actuator model

As previously mentioned the actuator model is not part of this thesis and for simulation purposes, simple actuator block is modelled to simulate the pressure through a simple on/off solenoid valve, while the input is the current from the control block. In the Figure 46 the simple on/off solenoids and the rail are shown. As a simplification for this model, assumption is made that only one valve is actuated during the movement towards the targeted gear.

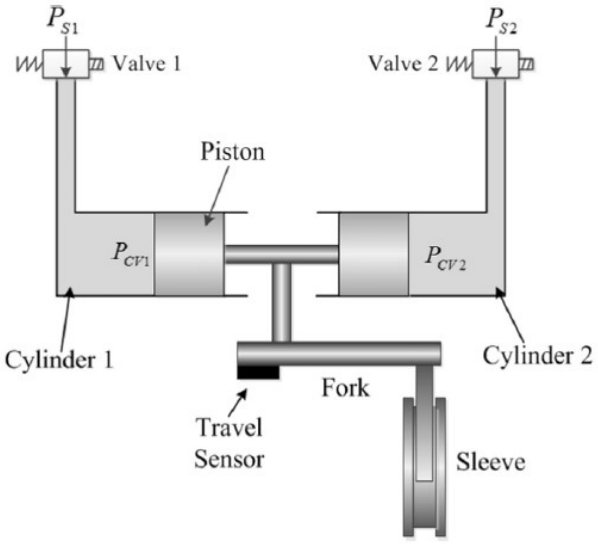

Figure 46 Simplified hydraulic actuator (15)

As already mentioned, the information about the geometry and specification is often classified and not easy to find. In (15) one diagram, Figure 47, shows the calibrated values

of the pressure through the solenoid valve as the function of the current on this on/off solenoid valve. This is used for modelling a look-up table in the model that represents the pressure through valve. The look-up table is created approximately to the diagram from Figure 47. Figure 48 further shows how the pressure of the piston area is calculated. Here it is visible that the maximal pressure is divided into the half so that the output of the pressure has the maximum of eight bar, which is the limit in the hydraulic pressure line for the DCT that is used as a subject of this thesis.

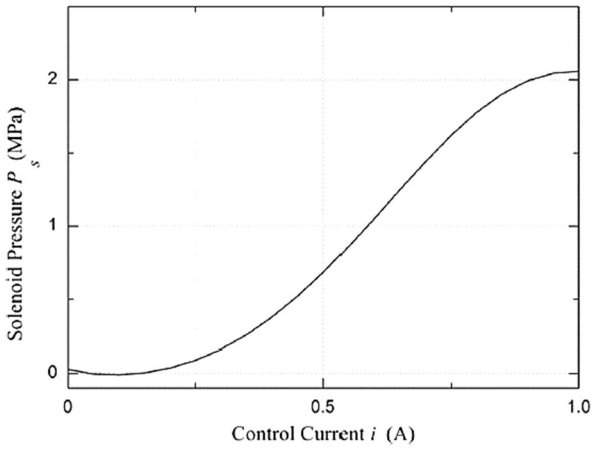

Figure 47 Solenoid calibrated current-pressure curve (15)

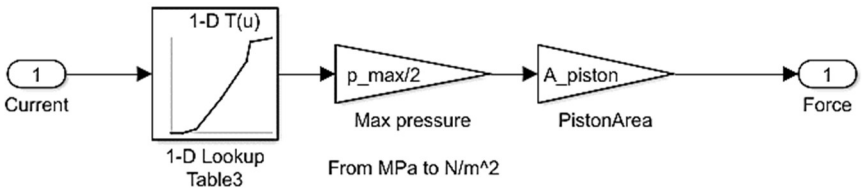

Figure 48 Simple force model

5.4 Parameters

The model for the rail used to engage two different gears, which is defined according to the following mathematical equations and physical laws, has lot of parameters that are hard to obtain from the manufacturers and were not all know at the time of the writing of this thesis. Even though some parameters were obtained, not all of them were from one manufacture or from the DCT that was used as a subject for previous sections of this thesis.

In this section all parameters for the model of one certain rail are listed in Table 2. All of these parameters are considered to be in international system of units, except for the parameter *p* for the pitch. All of the units for the parameters in this table are also described in beginning of this thesis.

PARAMETERS			
Actuator (15)			
A_{piston}	0,0007		
p_{max}	800000		
Synchronizer (2), (15)			
$x_{sleeve_{stop1}}$	0,0025	L_{spring}	0,04
$x_{sleeve_{stop2}}$	0,004	$L_{spring0}$	0,045
$x_{sleeve_{stop3}}$	0,0035	a	0,00015
$x_{sleeve_{in}}$	0,008	b	0,0695
α_c	8	R_c	0.041
μ_{fric}	0,08	S_1	0,5
n_g	28	S_2	5
$\mu_{chamfer}$	0,08	R_i	0.05
μ_{solid}	0,09	β	45
θ	45	p	10
k_{spring}	80	h_0	0.00001
m_f	0,3	m_s	0,2
n	3	h_{min}	0,000001
μ_v	0,02		
Clutch Drag Torque (15)			
r_2	0,106	h_{cd}	0,00041
μ_{cd}	0,0315	N	8
μ	0,07221	r_1	0,0965
r_m	0,10125		
Inertia (21)			
J_{11}	0,0023	J_{22}	0,0009
J_{33}	0,0023	J_{44}	0,0009
J_{55}	0,0023	J_{66}	0,0009
J_{77}	0,0023	J_{RR}	0,0009
$J_{outputshaft1}$	0,105	$J_{outputshaft2}$	0,105
Ratios (21)			
i_1	3,14	i_2 (15)	2,23
i_3 (15)	1,41	i_4	1,00
i_5	0,92	i_6	0,76

i_7	0,6	i_R	4,04

Table 2 Parameters

5.5 All rails

After the model for one certain rail that engages the gear from the neutral position was developed, implementation of the same rail model that can engage two gears was considered. With logic operators from the MATLAB Simulink toolbox it is possible to simulate different rail movement for all gears, while using targeted gear as input value. In DCT, one rail is always used for engagement of two different gears. This rail model considers only the movement starting from the neutral position, while the rail is stopped in neutral position. Due to the different geometry and design of the synchronizers for every rail, for each rail model it is necessary to adjust parameters. Furthermore, case block from the MATLAB Simulink library is used in order to calculate the correct rail movement. In Figure 49 the functional block diagram for simulation of all rails in DCT as mentioned above is illustrated.

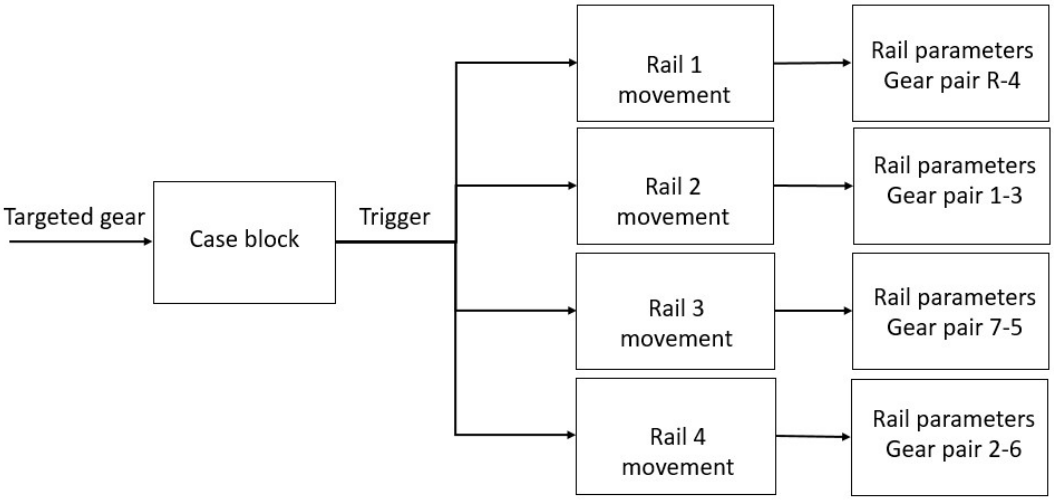

Figure 49 All rails

6. Rail Controller

Different sensors are assembled within a vehicle with DCT. For the rail control in the transmission, position sensor of the rail, opened and closed clutch speed and outputshaft speed can be used for the design of the rail control. Therefore, the control of the model is designed according to the available data from the vehicle.

6.1 Control logic

This plant model is characterized with nonlinear behaviour with different points of the discontinuity. From a physics perspective, it can be seen in theoretical analysis in previous chapters, that through movement of the rail, four different equations of the motion comprise this process. While it would be possible for one PID controller to control the gear engagement, this strategy could produce different unpleasant events like teeth clashing, noise and block-outs (26), (27).

Furthermore, in case of the usage of single controller for this process, it is hard to achieve the desirable system response due to the fact that different phases of the rail movement are described with different equations of the motion. The implementation of one PI controller for the rail movement with the results of the simulations will be discussed later. Due to the fact that there is more than one phase in the synchronisation process and between these phases there are also discontinuity points, separate controllers are considered for each of these phases.

The idea behind the physics based control of the model is to separate the phases of the synchronization, so that every phase is easily controllable, and so that fast shifting without gear clashing, noise, or block-outs is possible (15), (23), (27). Also due to the fact that during its lifecycle the wear of the synchronizers increases (which can influence early ring unblocking and desynchronization after the ring rotation), it is possible to avoid and control some of these undesired events. This control design is possible with the implementation of a Stateflow chart block, which can be used to switch from one controller to another; while different events occur. This type of controller is also called a supervisor controller, as mentioned in (15), where these types of system are also labelled as hybrid-systems. During the analysis of the physics it was determined that the dynamics and design of dual clutch transmission with wet clutches can be unfriendly or aggressive to the synchronizers. Figure 50 shows supervisor functional diagram.

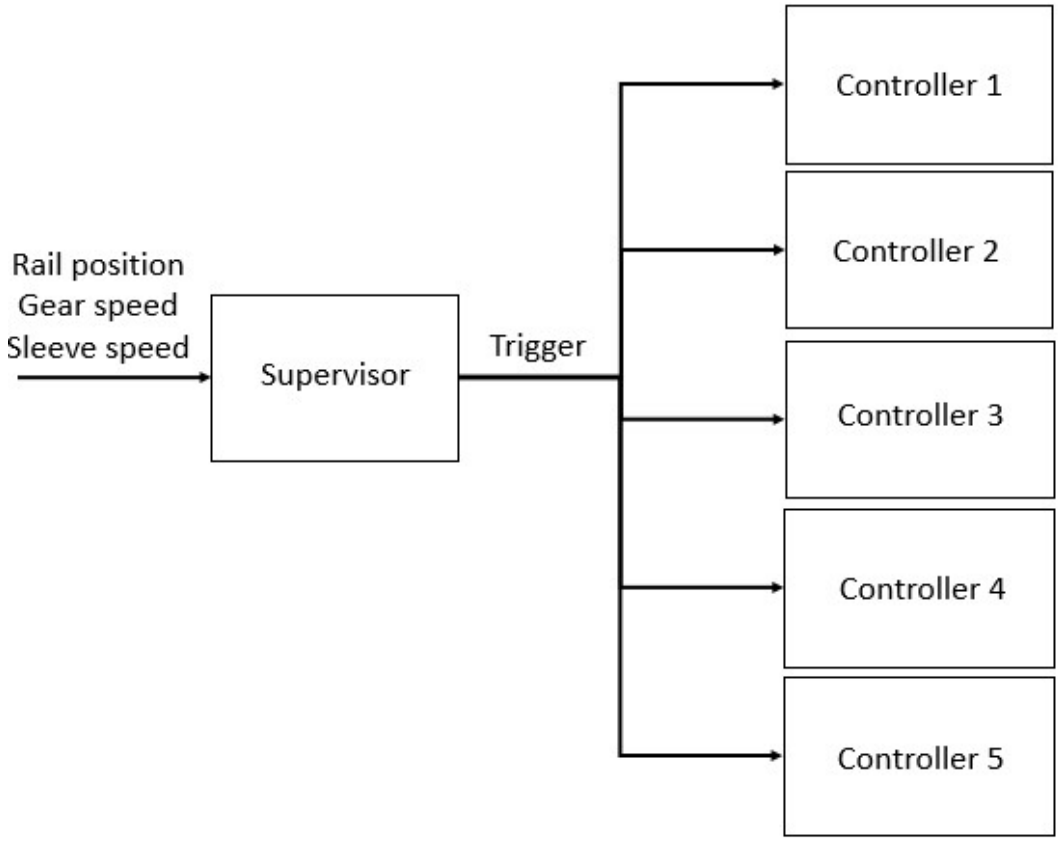

Figure 50 Supervisor control

The physics analysis of the synchronisation process has shown the importance of the pre-synchronisation phase, which allows the ring to get into the blocking position. It has also shown that an overly aggressive shift force can lead to ring unblocking before the gear has been synchronized, due to the stick-slip phenomenon and the wear of the ring cone surface over the lifecycle of the synchronizers. Therefore, for the pre-synchronisation phase (phase one) there should be enough time for the strut detent to set the synchronizing ring into the blocking position, while also the speed of the sleeve should not be too high so that the sleeve splines cause noise by clashing into the ring splines (15). During the synchronization phase, in order to have the fastest possible synchronization, the maximum force must be applied. As previously mentioned, different authors discussed the design of the synchronizers and the possibility of early ring unblocking during the synchronisation phase, due to the stick-slip phenomena and high oil viscosity at low temperature (20). Therefore, it has been considered that force maximum is not needed and not reached as soon as the sleeve and the gear get to the blocking position. For the phase three and the fly wheel phase, the sleeve should have higher velocity to ensure that there is not enough time for the desynchronization to happen, so that there is not any grinding sound. While approaching the top of the gear spline, the sleeve velocity must be reduced, so that the noise produced due to the bumping on to the gear splines for the start of the indexing phase is avoided.

The indexing phase has been identified as the main reason for the engagement noise and delays during the rail movement. As it has been described in previous chapters, the

initial alignment plays a major role in the indexing phase. It has been also shown that the initial alignment is random and not predictable. In the next chapter, the influence of the different alignment on to the rail movement will be discussed. Even though there is the ideal alignment where the rail movement can engage the gear with the least effort, there is not any possibility to control the initial alignment. As the author of (23) suggests, it is possible to detect bad alignment if the rail speed is equal to or less than zero. Also after the contact between the gear synchronization teeth and the sliding sleeve teeth has been established and the gear has been turned, for the final engagement the sliding sleeve velocity should be reduced to avoid clashing of the teeth with the end of the gear synchronization hub.

In the Stateflow chart there is also one output signal that shows whether the gear has been engaged. This is implemented as a display scope block where the values zero and one are displayed. If value one is displayed, the rail position for the gear engagement has been reached, and if the output is zero, there is failure in the synchronisation.

Figure 51 shows the supervisor control logic that is implemented in the Stateflow chart. At the start of the rail movement it is assumed that the rail is already in neutral position. Phase one, phase two, phase three, phase four, neutral, override and engaged blocks in this figure are describing different states in the Stateflow chart for the controller. These blocks output different trigger signals, that activate different controllers (Figure 50). The switching conditions for different controllers, as shown in Figure 51, are reached position of the rail, which also correspond to the switching conditions in the model Stateflow chart. Here, same as in Stateflow chart for the model, the switching condition for the next controller after the synchronization phase, phase two, is different. If the absolute speed difference between the gear and the sleeve is smaller than small value δ, state woud be changed to the phase three. After the supervisor switched to the controller for the indexing phase, another condition is implemented for the detection of the bad alignment as previously discussed. If the rail speed is less than or equal to zero, according to the author of (23) this could mean that the bad alignment or delays during the rail movement occur if the force for the rail movement is not high enough to turn the gear. This condition therefore switched to different controller, which will be discussed in the next section. Furthermore, another switching condition that is implemented from the phase 3 state will also be discussed in the last chapter.

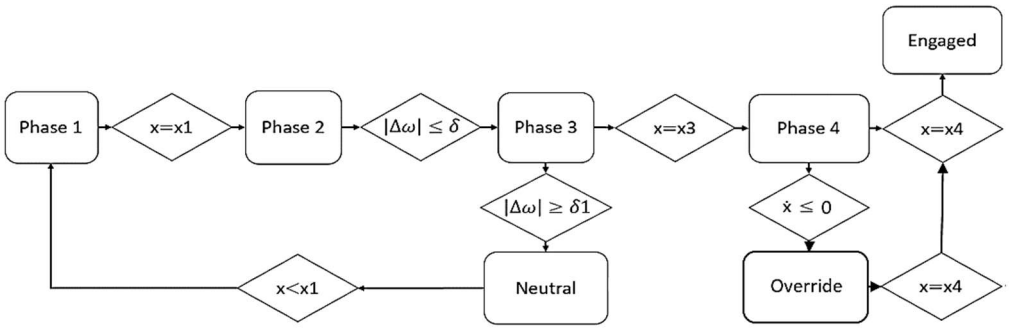

Figure 51 Controller state-machine logic

6.2 Controller

Each of the phases have different system dynamics and therefore, each phase has separate controllers implemented. The PI controller is chosen for phase one, phase three and phase four and neutral state, because it has a good response to the system dynamics and is easily tuneable with only two tuning factors. These controllers are feedback controllers, where they continuously calculate the error value as the difference between a desired set point and measured or calculated process variable and furthermore, apply corrections based on proportional and integrate terms. Therefore, PI-Controller stands for Proportional-Integrator Controller where the proportional term produces an output value where the error is then multiplied with the proportional gain constant. The integrator term in the PI Controller is described through integral, where all of the instantaneous errors over time are added, and the sum is multiplied by the integral gain constant (35). The output signal from the controller is the current that further flows to the actuator block. According to the current, pressure through valve is released and applied to the piston area, which further results into the shift force.

For these controllers it was necessary to tune them according to the given system they are designed to control. For this model for simulation purposes tuning was made manually while observing the system response to the step response, while the parameters of the PI controller were changed. For the phase one, where the rail position is controlled to reach the blocking position, the controllers are tuned so that the response does not have any overshoot, and so that the sleeve can smoothly come into the blocking position. The PI controllers for ring rotation are also tuned so that the rail reaches the position where the indexing is possible. Once again the controller is tuned so that there is no overshoot. In the last phase, the PI controller is tuned so that the gear is turned smoothly without reducing translational rail speed. As previously mentioned, for the synchronization phase, open loop control with predefined current output is chosen, so that fastest possible speed synchronization can be achieved. As the author of (27) suggests, it is also possible that PID controller with high gain parameters could be used here for the maximum force, but it is also suggested that the controllable increase of the synchronization force is more desirable in the start of the synchronization phase. Also for the override state, open loop control with predefined current output is used, so that the force can be rapidly increased if bad alignment occurs.

6.3 Simulation

The simulation of the rail control is performed using fixed-step solver. This solver is recommended from (36) as a solver for models that contain multiple switches and as a solver that can handle models that contain both continuous and discrete states. More information about the solver can be found in (36). Step size that is chosen for the simulation is 0.00001 and the solver is chosen automatically.

6.3.1 Results

As previously mentioned, different parameters are taken from different reference literature and used for the simulation purposes. Different simulations are performed for

upshift and downshift rail movement and different control possibilities are discussed for the same preselection process.

In Figure 53, Figure 54, and Figure 55 the results for first set of simulations are shown, whereby the first figure shows shift force during the rail movement, the second figure shows the rail position and the third figure shows the sleeve speed and the gear speed. The opened and closed clutch speed are set to be approximately like the authors of (15) used it in their work, for upshift and downshift. This figure order will be shown in all described results in this chapter. In these figures the results from certain simulation are plotted with the same colour in all these charts. Therefore, for example, the green colour from Figure 53, Figure 54 and Figure 55 corresponds to the same simulation results.

The first set of simulations are performed during a 3-2 downshift, while using only one PI to control the rail position. The PI parameters are equal for all of these simulations except for the simulation where *z*=0,1663, where the parameters are changed so that a higher force is applied. As previously mentioned, z variable describes different initial alignment between the gear and the sleeve teeth prior to the gear rotation. Furthermore, the comparison of the rail control for different reduced moments of inertia and different spring force is shown, while the influence of the alignment prior to the indexing phase has been identified.

The simulation results show that increased shift force for the gear engagement during the indexing phase is needed for gear rotation for the alignment, that is near the perfect alignment. The perfect alignment occurs when there is no relative gear rotation and the rail can reach the end position with least effort. Also, it can be seen that this alignment has more influence on the gear rotation than the alignment, where the sleeve does not need to turn the gear against the clutch drag torque. This corresponds to the works of other authors, such as (23), (31), and (30). Different gear rotational speed peaks are also shown in these figures after the gear speed and sleeve have been synchronized. These peaks are explained through geometry. In Figure 52 these peaks are caused through the sliding of the first touching point between sleeve chamfer and gear chamfer from position one to position two. Through this movement, the sleeve will move forward in straight line while the gear will be rotated. This rotation causes the speed peaks in the simulation results.

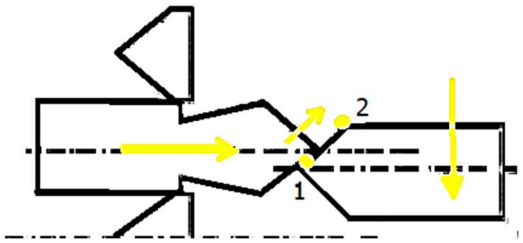

Figure 52 Speed peak

For the simulation results with z=-0,5032 the value of the spring force has been changed to be ten times larger than those for the simulation results with z=2,54. The results for the spring force variation show that during the pre-synchronization the controller compensates this change, while more force is applied on the rail pistons. Furthermore, it is notable that the synchronization phase time is shorter for the case where the spring force is increased. The simulation results with z=3,722 and z=0,871,

where the moment inertia is almost four times lower than it is with z=2,54 while other parameters remained unchanged, show that the synchronization time is reduced for almost 100 [ms] for lower moments of inertia.

In the Figure 54 the rail position is shown, while it can be seen that there is some delay during the start of the rail movement, because the shift force needed to be higher than the break through load. This is also caused by the controller, which is tuned so that smooth and slow movement is achieved, so that there is no bumping of the sleeve teeth on to the blocker ring. The simulations also show that the speed of the gear rotation is influenced by the indexing torque and the initial alignment as it can be seen in Figure 55. For different alignment different peaks of the gear speed can be observed. The reduction of synchronization time is also attempted by increasing the PI parameters to increase the shift force. The simulation results for this case show that the pre-synchronization phase ends almost instantly, while the force during the synchronization phase is not significantly higher. It is also shown that the controller during the indexing phase fails to control the rail. It can be seen that there are different difficulties for the rail control when a single controller is controlling the rail. It is hard to obtain correct parameters for the controller for the hybrid system as mentioned in (15), while in order to reduce the main synchronization phase, other events become uncontrollable and can create different noise and block out problems.

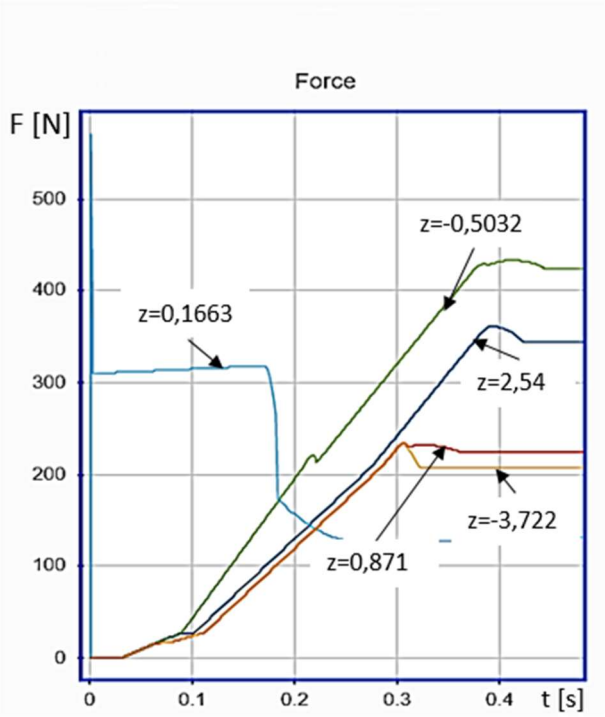

Figure 53 Downshift 3-2 Force - Single PI controller

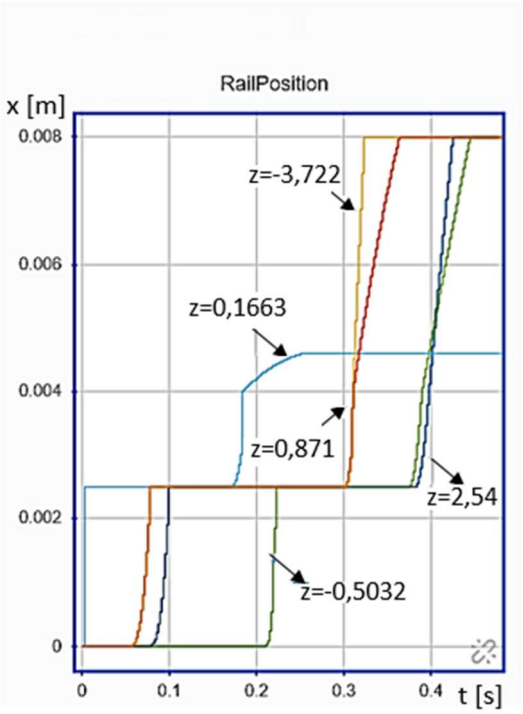

Figure 54 Downshift 3-2 Rail Position - Single PI Controller

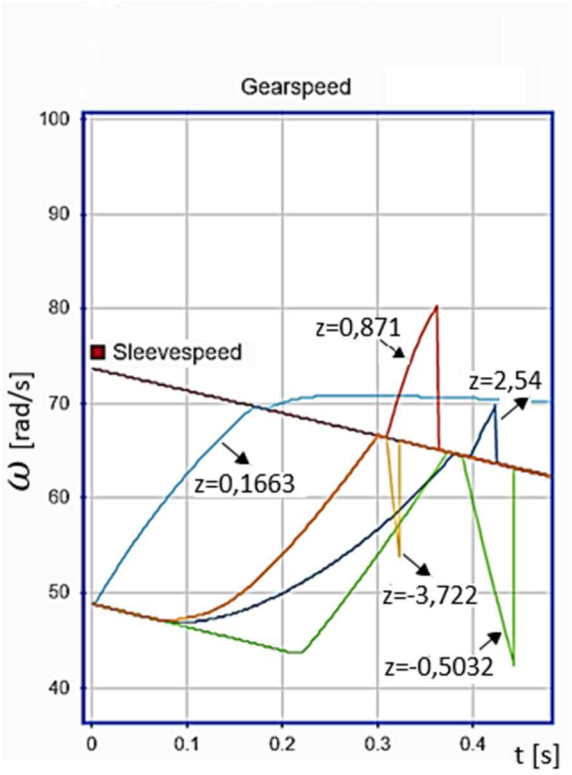

Figure 55 Downshift 3-2 Gear speed- Single PI Controller

The second set of the simulations is performed with an adaptive control with the supervisor as previously mentioned. The parameters that are used for these simulations can be taken from the previous chapter, where all parameters are declared in the

corresponding chapter. First, the focus is to get the highest possible force during the main synchronization phase, while different controllers and different parameters are used for other phases. For the phase one, PI controller is used. The goal for this phase is smooth transition to the blocking position. For the phase three and phase four also PI controllers are used, while for the override current output profile is chosen that allows only half of the force maximum.

The results in Figure 56, Figure 57, and Figure 58 show that by using the adaptive control it is possible to reduce the synchronization time while controlling every phase as separate system. It can be also seen that for this phase, the chamfer alignment has different influences on the shift force during the indexing phase. While in previous simulation set the alignment nearest to the ideal alignment also produced the most delay and the direction of the ring rotation did not play a significant role, here it can be seen that for the similar alignment the delay only occurs when the gear has to be turned opposite to the clutch drag torque. Here it is also visible that the override state in the supervisor control is active for the indexing phase. After the synchronization phase, where maximum force is applied, the force drops during the ring rotation and causes the sleeve to slow down. While the alignment in the start of the phase 4 is bad and the speed is already low, the sleeve stops and the override state is activated.

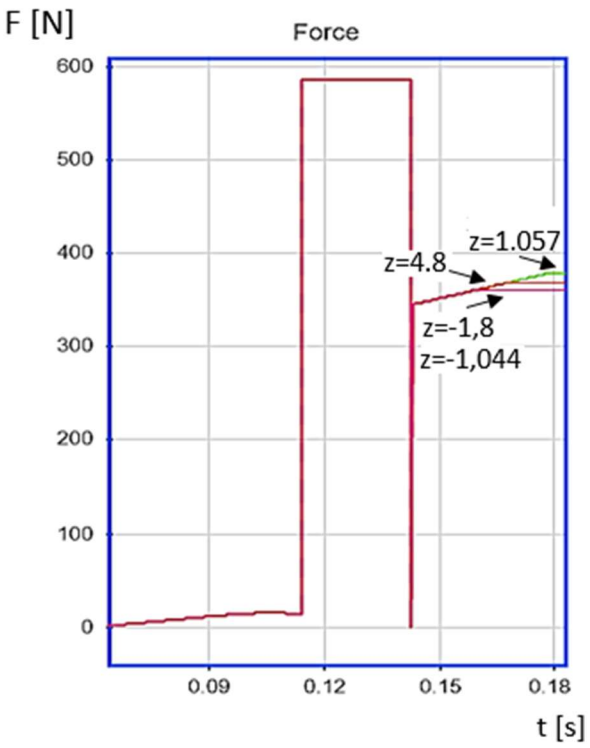

Figure 56 Shift force - Adaptive control - Set 1

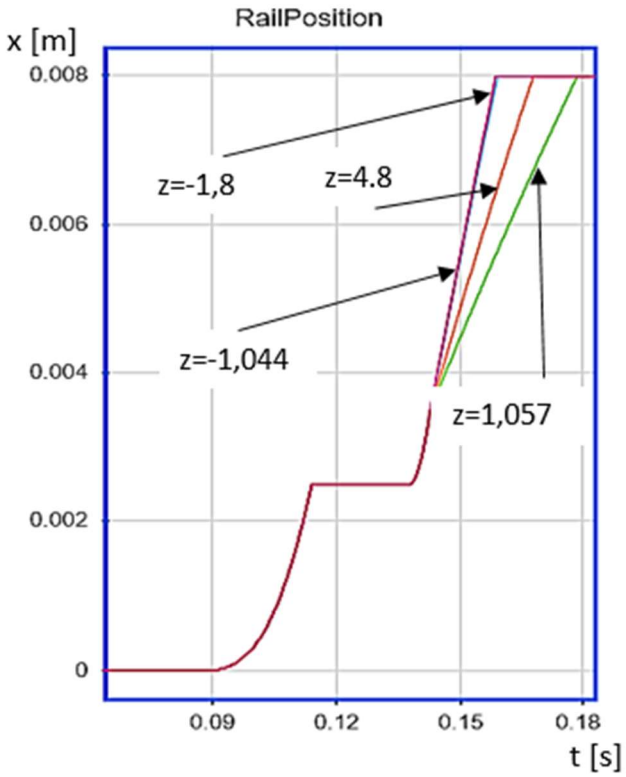

Figure 57 Rail position - Adaptive control - Set 1

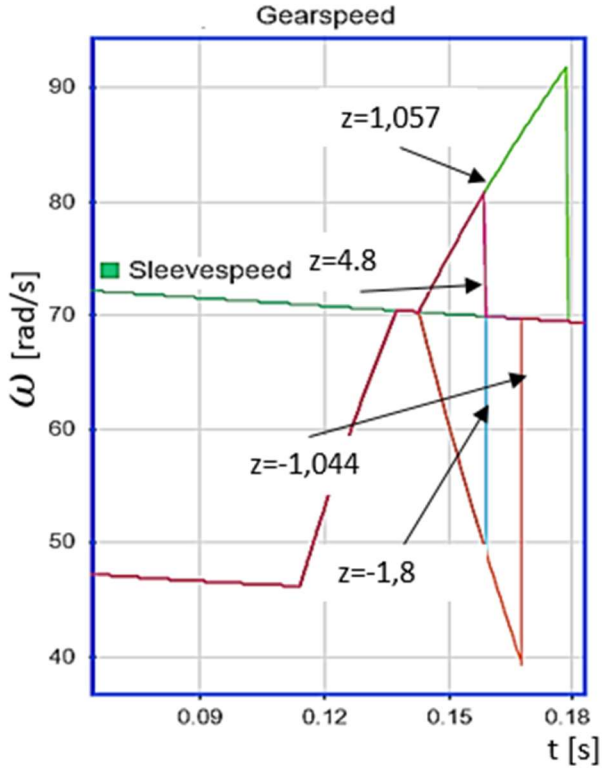

Figure 58 Gear and sleeve speed - Adaptive control - Set 1

Figure 59 and Figure 60 show the block out and delay in indexing phase when the override current profile is changed to z=1,79 (yellow line), compared to the previous simulation results with z=1,057 (green line). It can be seen that after the ring rotation and sleeve reaching the indexing position, there is not enough shift force to create indexing torque that high enough to turn the gear. Further, during the block out, noise issues could occur. (15)

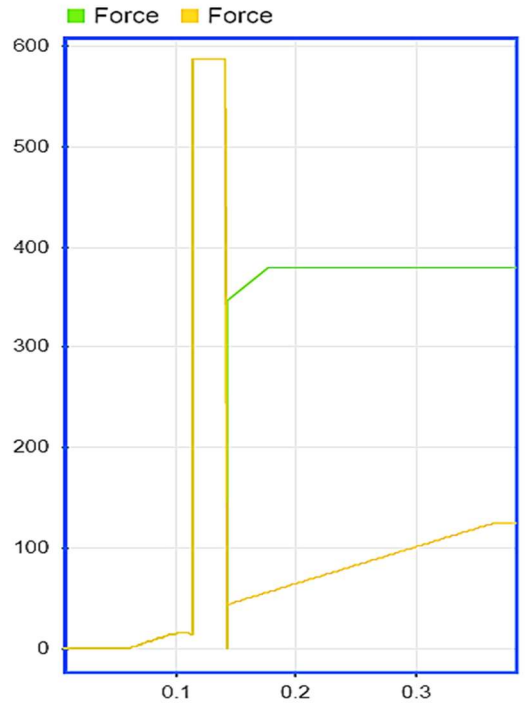

Figure 59 Shift force - Adaptive control - Block out

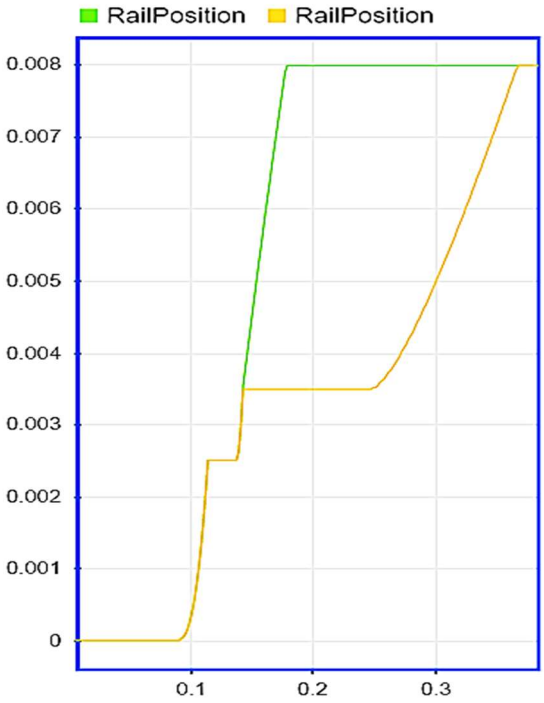

Figure 60 Rail Position - Adaptive control - Block out

For the next set of simulations, 2-3 upshift has been performed, with the same parameters as previously described. Furthermore, open loop control for the main synchronization phase has been introduced. Performance of the open loop is shown in Figure 61, Figure 62, and Figure 63. Because of the larger speed difference between sleeve and gear speed at the start of the main synchronization phase, the drag torque is also higher, which further prolongs the time of the synchronization. The goal of the open loop control is to have slower force increase, so that possible early ring unlocking can be avoided.

These figures also demonstrate the affection of the different open loop control strategies on the duration of the main synchronization phase. The unmarked (green line) simulation results shown in Figure 62 and Figure 63 indicate that, if the shift force increase is delayed, the duration of the synchronization time also increased accordingly. The simulation of the upshift process during these driving conditions shows that the proposed control also has certain delays if the controller is not tuned properly. Different difficulties also occur during the indexing phase. While for the downshift phase and different driving conditions the delays during this phase are reduced, for the upshift process there are still certain delays if the alignment is not friendly. For the rotation of the gear in opposite direction than the clutch drag torque and with bad alignment, the delay is almost 200 $[ms]$.

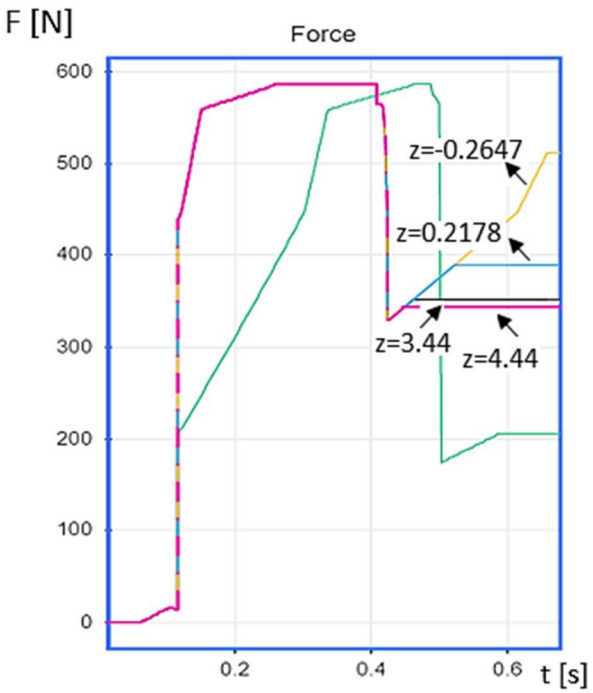

Figure 61 Upshift 2-3 Shift force adaptive control

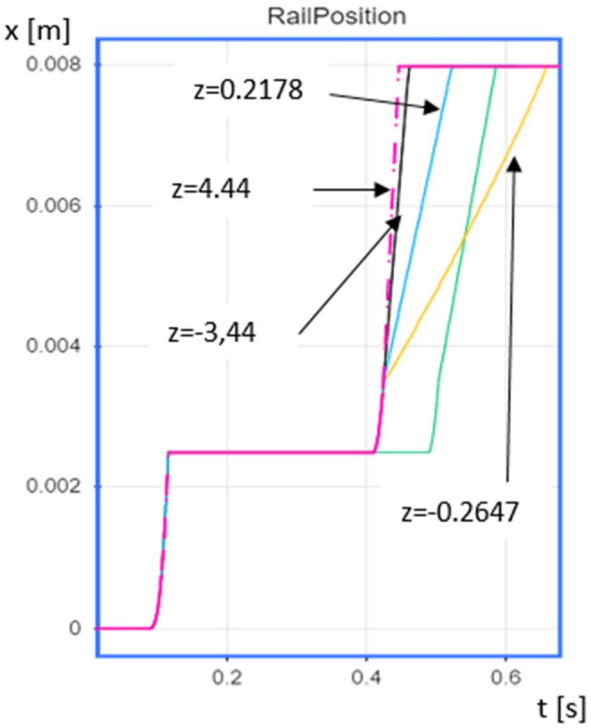

Figure 62 Upshift 2-3 Rail position adaptive control

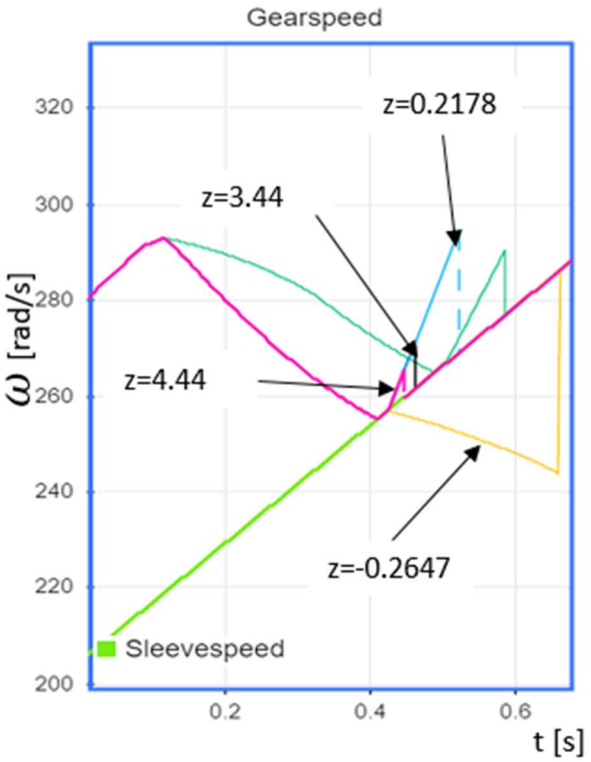

Figure 63 Upshift 2-3 Gear and sleeve speed adaptive control

It can be seen that delay issues in the rail movement are possible during the indexing phase, where if the force level is not high enough the sleeve cannot rotate the gear fast enough. In Figure 64, Figure 65, and Figure 66 different force levels for the indexing phase are compared to the previous results. Here the open loop control for the override state is changed, so that higher force is applied if bad alignment conditions occur. As it can be seen for similar alignment as in the previous results, the delays in the indexing phase are reduced with higher force level.

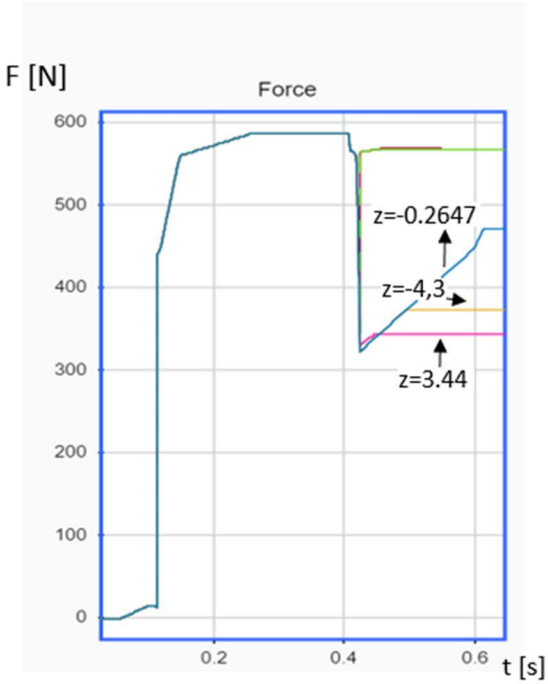

Figure 64 Upshift 2-3 Shift force adaptive control -different indexing

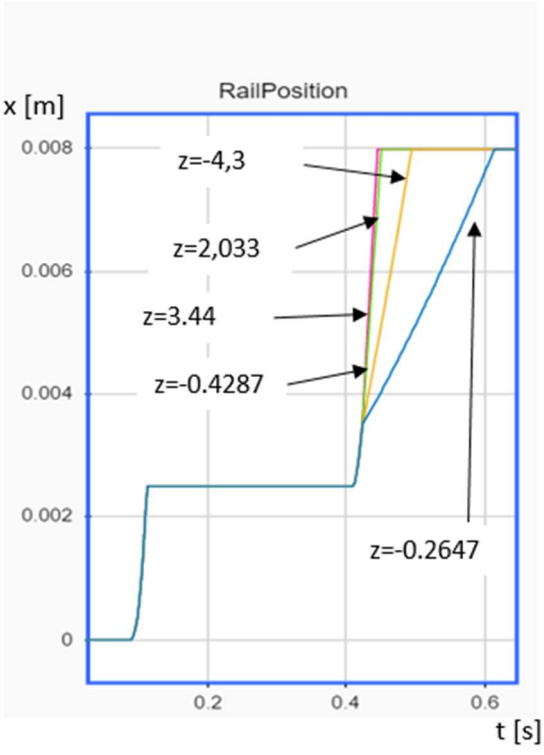

Figure 65 Upshift 2-3 Rail position - adaptive control - different indexing

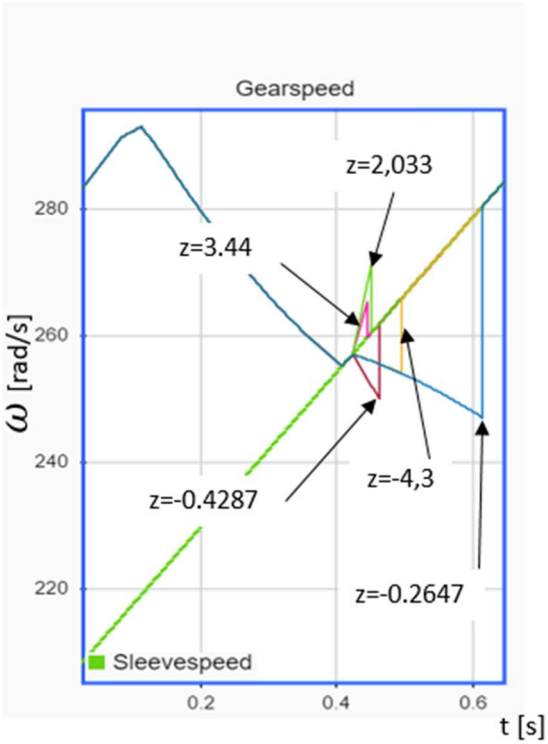

Figure 66 Upshift 2-3 Gear and sleeve speed - adaptive control - different indexing

7. Summary and conclusion

This thesis investigates gear preselection and engagement in dual clutch transmission (DCT). The investigation is described by the physical laws that occur in this process, whereby only the gear preselection in DCT that occurs on the opened clutch side is considered. Through the study of the rail and the gear preselection, the main problems during this process are enlightened, and the physics based equations are obtained. Through the separation of the system in actuator, synchronization body, and the interaction analysis, the control factors, and simplifications are obtained. Different authors describe the problems in the synchronization process for the manual transmission, while only a few of them consider dual clutch transmissions. The synchronization principle of dual clutch transmissions for the gear preselection is the same as in manual transmissions.

For the synchronisation process, eight phases are identified. Through simplifications, four main phase are extracted and the equations of the motion and the free body diagrams are introduced. Simulink is used for modelling and controlling of the rail within the four synchronization phases. In dual clutch transmission there are different factors that influence the synchronization process and the most important problem for the gear preselection is the drag torque. This torque is higher in dual clutch transmission due to clutch drag torque of wet clutches that are implemented in dual clutch transmissions and the fact that the preselection happens while the other part of the transmission is driven. The clutch drag torque is hardly measurable by direct measurement (15). Therefore, approximations have to be made for the drag torque model. In the present work, the drag torque model from Liu, explained in (15), is modelled.

The author of (26) mentions that in dual clutch transmission there are also different sources of vibrations that affect the synchronizers as well, because the preselection process generally occurs while the one clutch is driven. As it has been shown through the simulation process for upshift and downshift rail movement, the different delays can cause problems during the rail movement. Different cited reference literature explains that these delays can cause noise and failure in gear engagement. It has been shown that the force level after the synchronization between gear and sleeve speed has to be high enough so that the rail can overcome different alignment issues and engage the gear. In course of the investigation in this work, a new control strategy is presented, which is able to avoid gear clashing, early ring unblocking, and to controls different delays in the gear engagement. It is shown that control of the rail with one controller is not suitable, as this process is nonlinear and through the movement of the rail dynamics behaviour of the rail system changes rapidly. One PI or PID controller cannot predict this transient change behaviour. Therefore, the rail control has been divided into the different stages. This control strategy should be able to avoid grinding noise and to reduce time for gear engagement while maximal force for the synchronization process can be applied effectively with the target to also avoide clash of the splines with lower speed of the rail prior to the physical contact of the splines.

The goal of this master thesis is to develop a physics based control model for gear preselection in dual clutch transmission in MATLAB Simulink and also to develop the physics based control for this model, while also taking different sensors used in real vehicle applications into consideration. This is achieved successfully by identification of the main problems during the preselection phase of dual clutch transmission. In the work, many different parameters and effects, that affect synchronisation phase are identified, described and discussed. The introduced model can also be used to support design of the synchronizers. Furthermore, it can be used to assess energy consumption behaviour of the synchronization process to support investigations of the efficiency of synchronizers in dual clutch transmissions.

8. Limitations and future outlook

The physics based rail control model designed in this thesis can be used for the simulation of the gear shifting process in dual clutch transmissions. Different simplifications have been conducted while designing this model, wherein the emphasis was on the controllable parts of the rail. To enhance and verify the applied strategy, this model should be validated through implementation in a full vehicle model, and should be simulated by use of information from real test cases. The rail movement has been developed for the movement in positive direction toward the targeted gear and to simulate one gear engagement.

One of the limitations of the rail model is that in this thesis only one rail has been modelled. Different parameters have to be changed, in order to use this model for other rails. Before application in actual development processes, the control strategy that is implemented in this plant model should be validated with data from on-board vehicle tests.

Another limitation of this model is that, as previously mentioned, this model does not consider the static friction model and the desynchronization condition in the fly wheel phase. As other authors suggest, that there is possibility that this event occurs, it is possible to enhance the introduced model by implementation of an abort condition into the control supervisor. This condition observes the speed difference between the gear and sleeve speed and allows the sleeve movement toward indexing phase if the speed difference is not higher than 1 $\frac{rad}{s}$. This value has been proposed out of experience at the industrial partner and cannot be confirmed through the literature, except for (15), where it is clear that the gear engagement is possible even when speed difference is present. Another limitation of this model is that there is no output value that can explain noise and gear clashing. Here it is just assumed, as authors of (15) suggest, that delays during different phases could cause gear clashing and noise. Therefore, for further analysis and rail control, bumping models between the sleeve teeth with the ring teeth and gear teeth could be included. This control should be also tested with different actuator models, where the dynamics behaviour of the actuator is included.

8.1 Sync-free gear engagement in DCT

Currently in DCT the gear-change-strategy is only implemented in the way that the TCU gives a command so that the gear should be changed at some point where the clutch is opened so that the gear can be preselected for the point where the clutch should be closed for the transmission.

Mechanically, this means that the gear engagement is completed as in the manual transmissions where the gear shifting process is completed with synchronisation of the gear and the sleeve-body speed. In the synchronisation process the gear is slowed (accelerated) by the friction slip between two cone surfaces – the gear cone and ring cone. This process produces heat and wear of these two surfaces, which are one of the influencing factors for the durability behaviour of the gearbox parts, which may cause failures and noise in the gearbox.

While in the manual transmission it is impossible to know the current speed of the sleeve and the gear (there are no sensors installed), in DCT there are sensors that track opened and closed clutch rotational speeds, which can be later recalculated to the gear and sleeve speed, so that at in every operation point it is possible to calculate (track) all rotational speeds of all sleeves, clutches, and gears.

Because of the dynamics in DCT and the fact that there are two clutches and two drive shafts, there is a point in the operation cycle where the gear (ω_{gear}), which should be engaged, and the synchronisation body with the sleeve (ω_{sleeve}) are already rotating at the same speed. This is schematically illustrated in Figure 67.

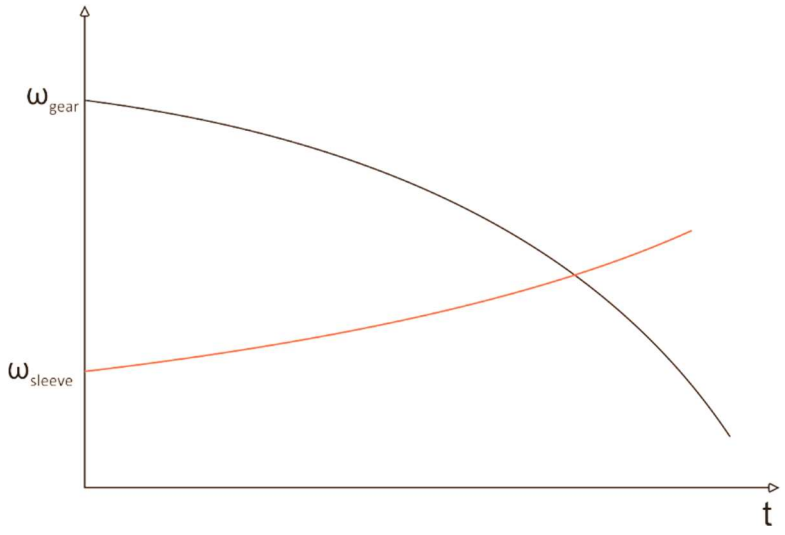

Figure 67 Gear and sleeve speed cross section over time

While the sleeve is rotating always with the speed of the output shaft multiplied with the current gear ratio, the gear that should be engaged as the next one is currently on the other shaft, which is closed at some point but continued to rotate through inertia or if there is already another gear engaged, which causes rotation of the opened clutch shaft. The sensor of the opened clutch tracks the rotation speed of this clutch and this speed times the gear ratio of the speed that should be synchronised is the speed of the gear.

In the illustrated example, the sleeve speed of the synchronisation body, which will be used to engage the next gear, is accelerating and the gear that should be engaged is slowing and fly wheeling (opened clutch rotation speed times gear ratio of the gear to be preselected).

At some point of the process, the speed difference will be zero and, because the speed will be already synchronised, the synchronisation time will be reduced, while the slip between the cones will be approximately zero. The simulation results performed with the adaptive control, shown in Figure 68 and Figure 69, demonstrate that the clutch drag torque influences the main synchronization process. It can also be seen that, for this strategy, the alignment between the gear and sleeve splines influences the rail movement, where short delay is not avoidable. Nevertheless, the main synchronization time for the proposed strategy, whereby the friction torque accelerates the speed, was reduced to a value below 20 $[ms]$. Furthermore, the force level needed to complete the engagement remained approximately the same, but the time needed to complete the synchronization was reduced to approximately 40 $[ms]$.

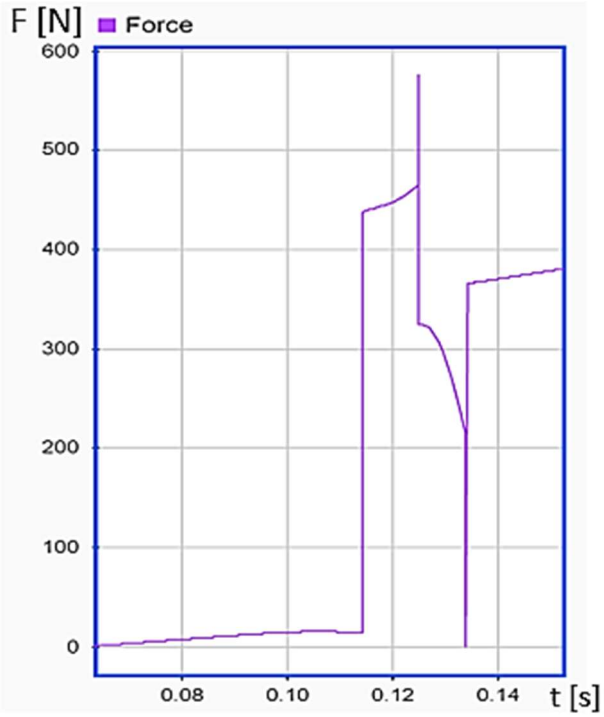

Figure 68 Novel strategy - shift force

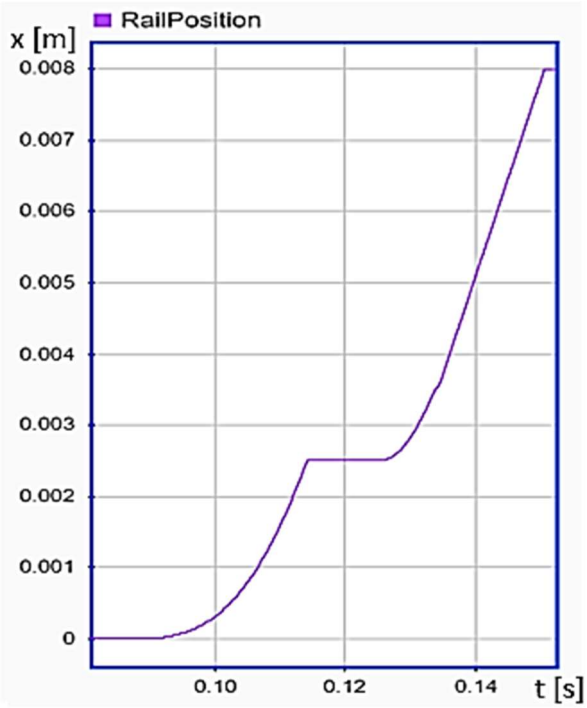

Figure 69 Novel strategy - rail position

8.2 Advantages

The hypothesis above can be used to optimize the gear preselection so that, through this strategy of the gear engagement, the wear and heat production can be lowered, which might increase the durability of the ring and the gearbox functionality. On the other hand, the synchronisation time of the gear and the sleeve can be reduced to a minimum. Even though the force level should remain the same so as to complete the engagement, the time lapse during which shift force is applied can also be reduced due to the shorter synchronization time, so that the power consumption might be also lower.

Bibliography

1. Harald Naunheimer, Bernd Bertsche, Gisbert Lechner. *Fahrzeuggetriebe.* Leipzig : Springer-Verlag Berlin Heidelberg, 2007. 978-3-540-30625-2.

2. Bedmar, Ana. *Synchronization processes and synchronizer mechanisms in manual transmissions.* [date of access: 20170805.] Göteborg, Sweden : CHALMERS UNIVERSITY OF TECHNOLOGY, 2013.

3. statista. [Online] [date of access: 20171113.] https://www.statista.com/statistics/204123/transmission-type-market-share-in-automobile-production-worldwide/.

4. Jinsung Kim, Kwanghyun Cho, and Seibum B. Choi. *Gear Shift Control of Dual Clutch Transmissions with a Torque Rate.* [date of access: 20180115.] San Francisko, USA : American Control Process, 2011. 978-1-4577-0079-8/11/$26.00 ©2011 AACC.

5. Sooyoung Kima, Jiwon Ohb, Seibum Choi. *Gear shift control of a dual-clutch transmission using optimal control allocation.* [date of access: 20180115.] s.l. : Department of Mechanical Engineering, Korea Advanced Institute of Science and Technology.

6. Manish Kulkarni, Taehyun Shim, Yi Zhang. *Shift dynamics and control of dual-clutch transmissions.* [date of access: 20170520.] s.l. : Elsevier, 2006. 0094-114X/$.

7. Gühmann, Henrik Isernhagen Clemens. *Modelling of a Double Clutch Transmission with an Appropriate Controller for the Simulation of Shifting Processes.* [date of access: 20170520.] Berlin : The Modelica Association, 2008.

8. A.Wood, David. Car complaints. [Online] 5 3 2017. [date of access: 20171029.] https://www.carcomplaints.com/news/2017/ford-dual-clutch-transmission-lawsuit.shtml.

9. Sedgwick, David. Automotive news. [Online] 7 12 2015. [date of access: 20171029.] http://www.autonews.com/article/20151207/OEM06/312079988/once-promising-dual-clutch-transmissions-lose-favor-in-u.s..

10. Robert Fischer, Gunter Jürgens, Ferit Kücükay, Rolf Najork, Burkhard Pollak. *Das Getriebebuch.* Wieb : Springer, 2012.

11. AG, Volkswagen. Direct Shift Gearbox, Self-Study Programme. [date of access: 20170420.] Wolfsburg : s.n., 10/2003. Vol. 000.2811.29.20 Technical status 10/03.

12. Adhitya, Mohammad. *A New Control Strategy of Wet Dual Clutch Transmission (DCT) Clutch and Synchronizer for Seamless Gear Preselect .* [date of access: 20171120.] s.l. : SAE, 2013.

13. Olivi, Davide. *Development of control-oriented models of Dual Clutch Transmission systems.* [date of access: 20170420.] Bologna : Alma Mater Studiorum – University of Bologna, 2013. ING-IND/08 – FLUID MACHINES.

14. T.Razzacki, Syed. *Synchronizer Design and Development for Dual Clutch Transmission (DCT).* [date of access: 20170520.] Detroit, USA : 2007 SAE International, 2007. 2007-01-0114.

15. Tongli Lu, Hongkui Li, Jianwu Zhang, Hongtao Hao. *Supervisor control strategy of synchronizer for wet DCT based on online estimation of clutch drag torque.* [date of access: 20170520.] s.l. : Elsevier, 2015.

16. ImageTransmission. [Online] [date of access: 20180115.] http://image.slidesharecdn.com/manualtransmissionsysteminautomobiles-130419085843-phpapp02/95/manual-transmission-system-in-automobiles-10-638.jpg?cb=1379378031.

17. team-bhp. [Online] [date of access: 20171020.] http://www.team-bhp.com/forum/attachments/technical-stuff/1420447d1443404564-ford-powershift-dual-clutch-transmission-dct-technical-overview-output-shafts.gif.

18. Manyala, John. *Gearshift Actuator Dynamics Predictions in a Dual Clutch Transmission.* [date of access: 20170520.] s.l. : SAE International, 2013. 10.4271/2013-01-9021.

19. Uwe Wagner, Reinhard Berger, Matthias Ehrlich, Manfred Homm. *Electromotoric actuators for double clutch transmissions.* [date of access: 20180220.] s.l. : LuK SYMPOSIUM, 2006.

20. Back, Ottmar. *Basics of synchronizers.* [date of access: 20180115.] s.l. : Hoerbiger, 2013.

21. SASTE, SAURABH. *ANALYTICAL AND KINEMATIC ANALYSIS OF THE SYNCHRONISER for Direct Shift Gearbox.* [date of access: 20180115.] Bradford : University of Bradford, 2013.

22. *Zwischenringe für Mehr-konus-synchronisation.* INA-Schaefler KG. Automobil Product Information, [date of access: 20180321.] s.l. : mandelkow GmbH, 2002, Vol. API6.

23. Paul D. Walker, Nong Zhang. *Engagement and control of synchroniser mechanisms in dual clutch transmission.* [date of access: 20170520.] Sydney : ElsevierLtd., 2011.

24. *Failure of Synchronization In A Manual Gearbox.* Goga, H. Szöky – J. Murin - V. 10, [date of access: 20171020.] Bratislava : Journal of Engineering IOSRJEN, 2014, Vol. 4. 2278-8719.

25. Paul Walker, Nong Zhang. *Parameter study of synchroniser mechanisms applied to dual clutch transmissions.* [date of access: 20170520.] 2014.

26. Paul D.Walker, NongZhang. *Investigation of synchroniser engagement in dual clutch transmission.* [date of access: 20170520.] Sydney : Elsevier, 2011. 10.1016/j.jsv.2011.11.005.

27. Gustavsson, Andreas. *Development and Analysis of Synchronization Process Control Algorithms in a Dual Clutch Transmission.* [date of access: 20180115.] Linköping : Linköping universitet, 2009. LITH-ISY-EX--09/4191--SE.

28. *Modelin, analysis and constraned control of wet cone clutch systems: A synchromesh case study.* Hossein Bahid Alizadeh, Mohamed K. Helwa, Benoit Boulet. [date of access: 20180115.] Toronto : Elsevier, 2017. 0957-4158.

29. Hongkui Li, Tongli Lu, Jianwu Zhang and Hongtao Hao. *Modelling and analysis of the synchronization process for a wet dual-clutch transmission.* [date of access: 20170520.] s.l. : IMechE, 2015. 10.1177/0954407015575856.

30. *Mechanical behaviour simulation for synchromesh mechanism improvements.* L. Lovas, D. Play, J. Marialigeti, J. F. Rigal. [date of access: 20170920.] Budapest/ Lyon : IMechE, 2006, Vol. 220. 10.1243/0944070D21604.

31. *Modelling of gear changing behaviour.* L.Lovas, D.Play, J.Marialigeti, J.F. Rigal. [date of access: 20170920.] Budapest : PERIODICA POLYTECHNICA , 2005. PP. 35–58.

32. Paul D. Walker, Nong Zhang, Ric Tamba, Simon Fitzgerald. *Simulation of dra torque affecting synchronizers in a dual clutch transmission.* [date of access: 20170520.] s.l. : Springer Verlag, 2011.

33. MATHWORKS. Mathworks/Simulink. *SIMULINK.* [Online] MATHWORKS. [date of access: 20180201.] www.mathworks.com/help/simulink/index.html.

34. Mathworks Stateflow. *Stateflow.* [Online] Mathworks. [date of access: 20180202.] https://de.mathworks.com/products/stateflow.html.

35. Wikipedia. Wikipedia PID. *PID Controller.* [Online] 2018 1 26. [date of access: 20180502.] https://en.wikipedia.org/wiki/PID_controller#PI_controller.

36. Mathworks/Simulink/Types of Solvers. *Documents.* [Online] Mathworks. [date of access: 20180201.] https://de.mathworks.com/help/simulink/ug/types-of-solvers.html.

37. Haas, Maximilian Johann. *Modellierung, Simulation und Sensitivitätsanalyse eines hydraulischen Schaltkreislaufes .* Graz : FH Joanneum, 2015.

38. Christopher Jay Weingartz, Glenn W. Hoefflin. *Verfahren zum Steuern einer Synchronisierungseinrichtungs-Aktuatorgabel eines Getriebes .* [date of access: 20180314.] *DE102015105280A1* Germany, 22 10 2015.

Appendix

Rail 1 Architecture

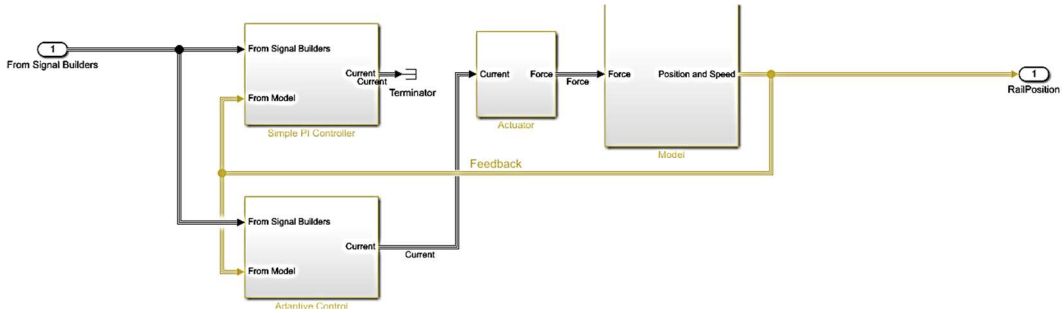

Model

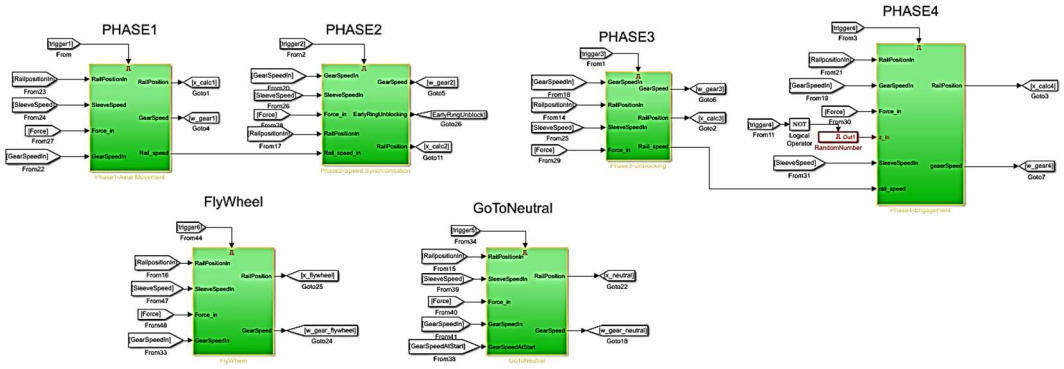

Axial movement of the sleeve in phase 1

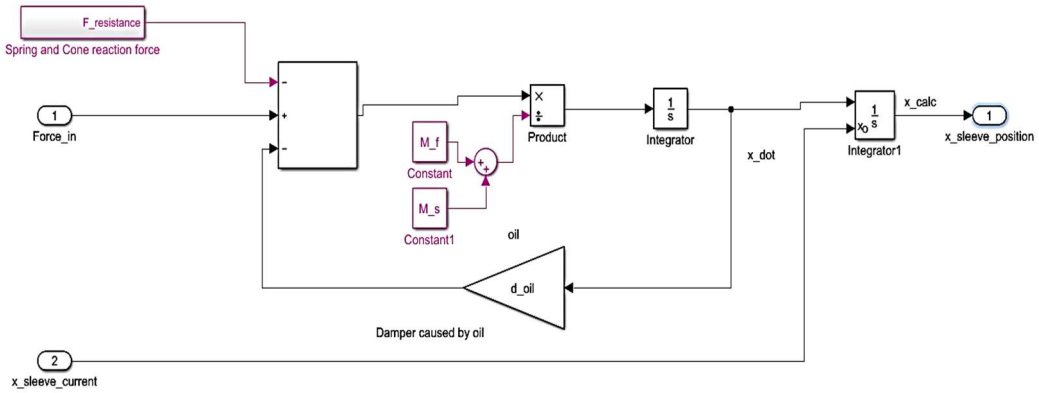

Rotational movement of the gear in phase 1

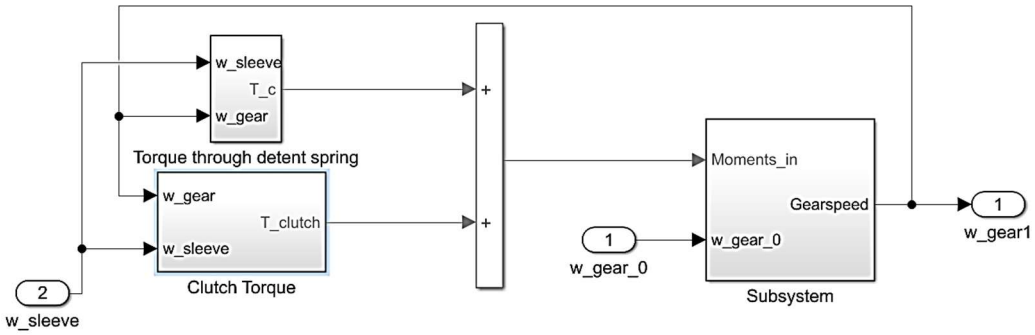

STATEFLOW model logic

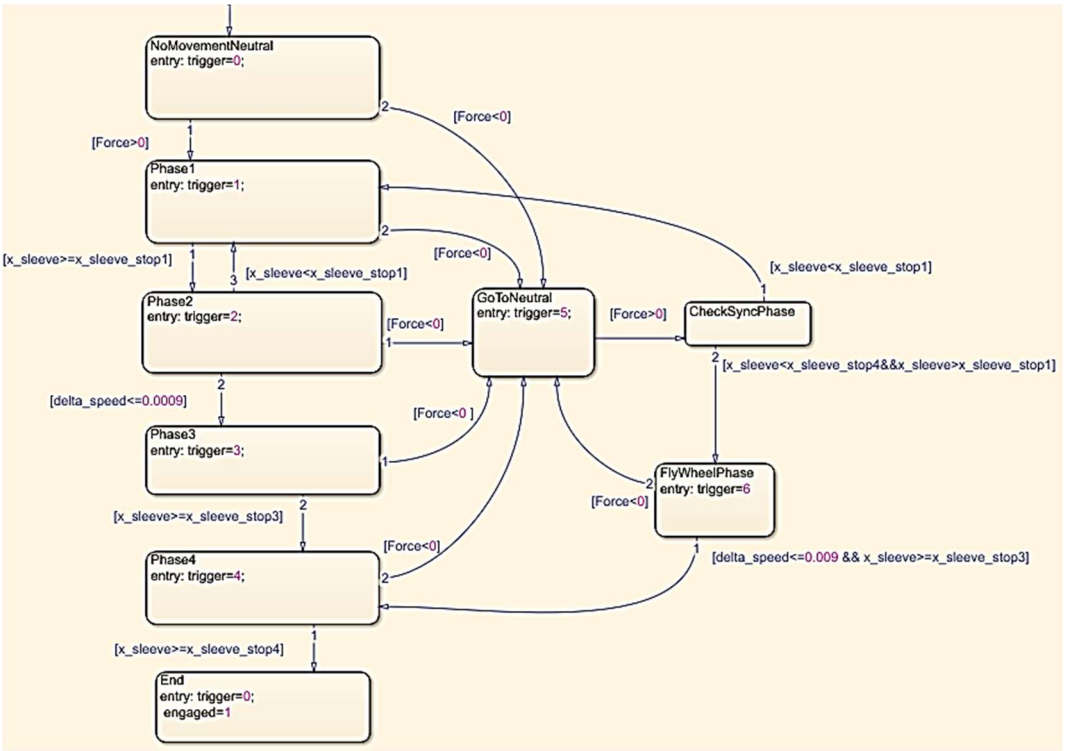

Triggers logic

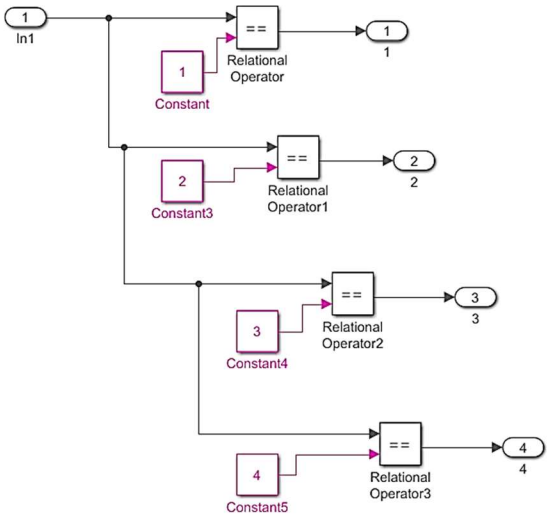

STATEFLOW Control logic

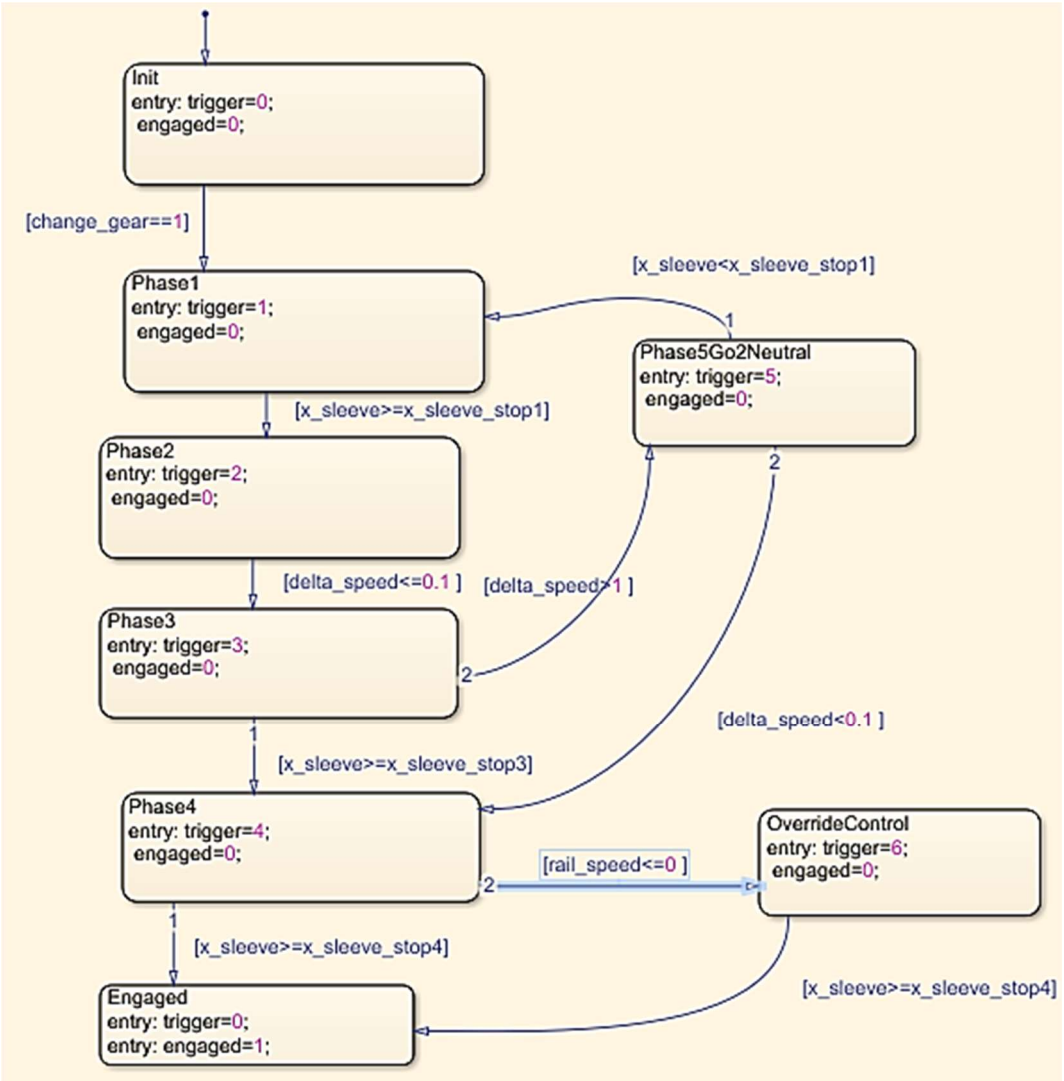

All rails control